JOC*Article*

# Determination of the Absolute Configurations of Natural Products via Density Functional Theory Calculations of Vibrational Circular Dichroism, Electronic Circular Dichroism and Optical Rotation: The Schizozygane Alkaloid Schizozygine

Philip J. Stephens*, Jian-Jung Pan, and Frank J. Devlin

*Department of Chemistry, University of Southern California, Los Angeles, California 90089-0482*

Marie Urbanová

*Departments of Physics and Measurements and of Analytical Chemistry, Institute of Chemical Technology, Prague, Technicka 5, 16628 Prague, Czech Republic*

Josef Hájíček

*Synthesis Development Group II, R&D Division, Zentiva, a.s., U Kabelovny 130, 10237 Prague 10, and Department of Organic and Nuclear Chemistry, Faculty of Science, Charles University, Hlavova 8, 12840 Prague 2, Czech Republic*

*pstephen@usc.edu*

*Received December 14, 2006*

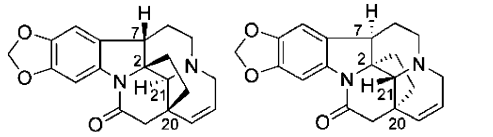


(2R,7S,20S,21S)-**1** OR (2S,7R,20R,21R)-**1** ?

The development of density functional theory (DFT) methods for the calculation of vibrational circular dichroism (VCD), electronic circular dichroism (ECD), and transparent spectral region optical rotation (OR) has revolutionized the determination of the absolute configurations (ACs) of chiral molecules using these chiroptical properties. We report the first *concerted* application of DFT calculations of VCD, ECD, and OR to the determination of the AC of a natural product whose AC was previously undetermined. The natural product is the alkaloid schizozygine, isolated from *Schizozygia caffaeoides*. Comparison of DFT calculations of the VCD, ECD, and OR of schizozygine to experimental data leads, for each chiroptical technique, to the AC 2*R*,7*S*,20*S*,21*S* for the naturally occurring (+)-schizozygine. Three other alkaloids, schizogaline, schizogamine, and 6,7-dehydro-19$\beta$-hydroxyschizozygine, have also been isolated from *S. caffaeoides* and shown to have structures closely related to schizozygine. Assuming a common biosynthetic pathway, their ACs are defined by that of schizozygine.

## Introduction

The alkaloid schizozygine[1−5] is one of a group of alkaloids that have been isolated from the East African plant *Schizozygia caffaeoides* (Boj.) Baill., belonging to the Apocynaceae family, which has been used in traditional medicine in Kenya for treatment of skin diseases.[5] Others include schizogamine,[1,2] schizogaline,[1,2] isoschizogamine[1,2,6,7] and isoschizogaline.[1,2,5] Schizozygine was first isolated and structurally characterized,

(1) Renner, U.; Kernweisz, P. *Experientia* **1963**, *19*, 244−246.
(2) Renner, U. *Lloydia* **1964**, *27*, 406−415.
(3) Renner, U.; Fritz, H. *Helv. Chim. Acta* **1965**, *48*, 308−317.
(4) Hesse, M.; Renner, U. *Helv. Chim. Acta* **1966**, *49*, 1875−1899.
(5) Kariba, R. M.; Houghton, P. J.; Yenesew, A. *J. Nat. Prod.* **2002**, *65*, 566−569.
(6) Hájíček, J.; Taimr, J.; Budesinsky, M. *Tetrahedron Lett.* **1998**, *39*, 505−508.
(7) Hubbs, J. L.; Heathcock, C. H. *Org. Lett.* **1999**, *1*, 1315−1317.

10.1021/jo062567p CCC: $37.00 
Published on Web 03/06/2007

**TABLE 1. Calculated Relative Energies (Δ*E*),[a] Relative Free Energies (Δ*G*),[a] and Percentage Populations (*P*)[b] of the Conformers of 1**

| | MMFF 94 | B3LYP/6-31G* | | | B3LYP/TZ2P | | | B3PW91/TZ2P | | |
|---|---|---|---|---|---|---|---|---|---|---|
| conformer | Δ*E* | Δ*E* | Δ*G* | *P* (%) | Δ*E* | Δ*G* | *P* (%) | Δ*E* | Δ*G* | *P* (%) |
| **1a** | 0.00 | 0.000 | 0.038 | 36.20 | 0.000 | 0.029 | 35.13 | 0.000 | 0.020 | 35.59 |
| **1a′** | | 0.011 | 0.000 | 38.62 | 0.023 | 0.000 | 36.89 | 0.030 | 0.000 | 36.82 |
| **1b** | 1.69 | 0.371 | 0.670 | 12.46 | 0.331 | 0.589 | 13.63 | 0.336 | 0.577 | 13.88 |
| **1b′** | | 0.365 | 0.658 | 12.72 | 0.307 | 0.559 | 14.35 | 0.316 | 0.585 | 13.71 |

[a] In kcal/mol. [b] Populations are based on Δ*G* at $T = 298.15$ K.

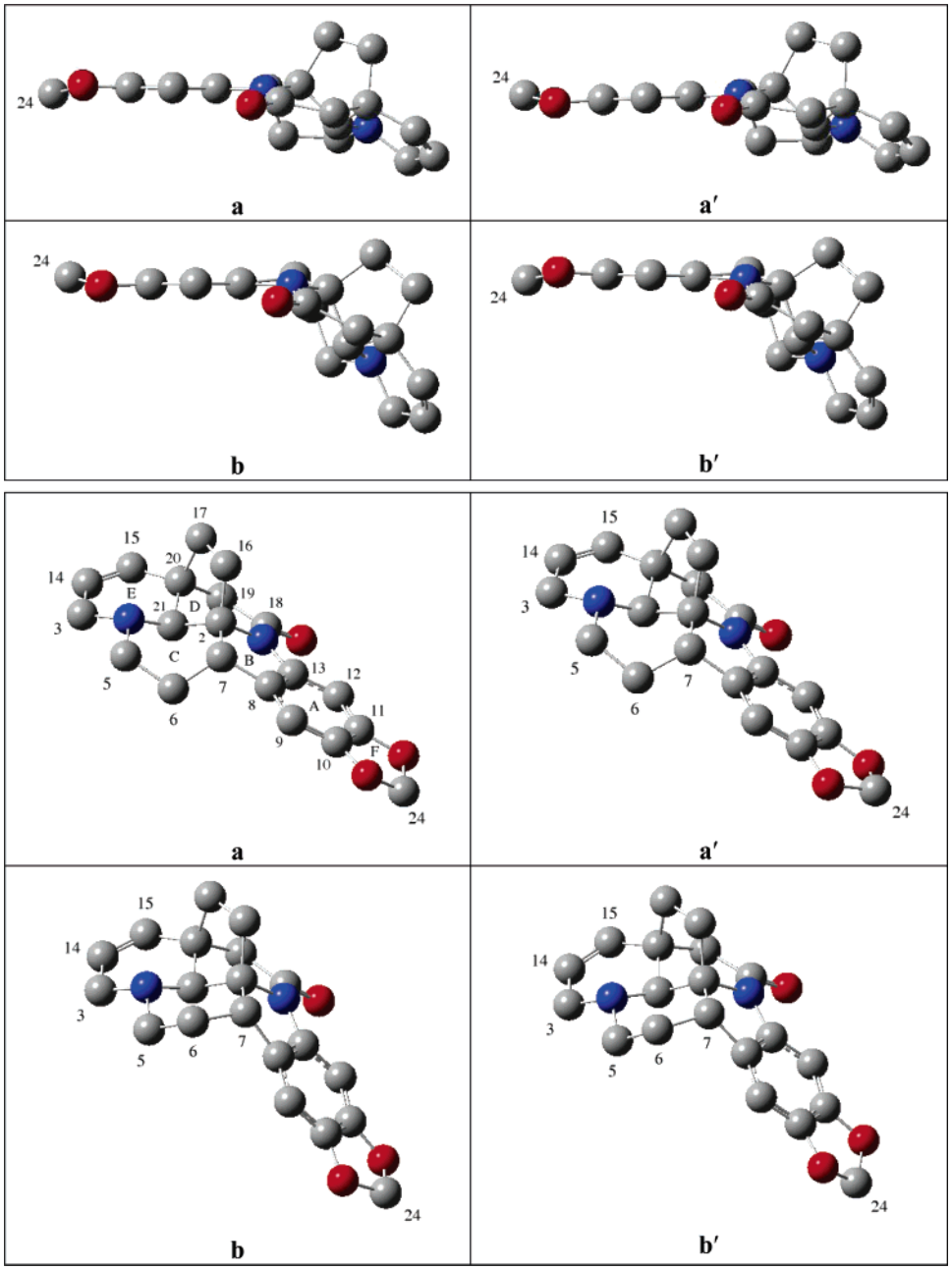


**FIGURE 1.** B3PW91/TZ2P structures of the four conformations of (2*R*,7*S*,20*S*,21*S*)-**1**.

via its chemical reactions and spectroscopic properties, by Renner and co-workers.[1−4] The structure deduced was **1**.

The chirality of this structure is consistent with the nonzero optical rotation of schizozygine: $[\alpha]_D = +15.5$ ($CHCl_3$).[1] The naturally occurring (+)-schizozygine can have either the absolute configuration (AC) 2*R*,7*S*,20*S*,21*S* or 2*S*,7*R*,20*R*,21*R*. To date, the AC of schizozygine has not been determined.

The structures of other alkaloids from *S. caffaeoides*, the "schizozygane alkaloids", have also been characterized.[5−7] In the case of isoschizogamine, total synthesis of the racemate has

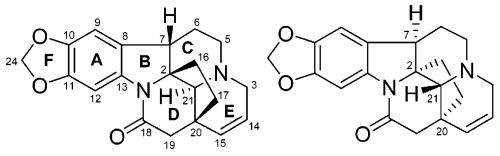

(2R,7S,20S,21S)-**1** (2S,7R,20R,21R)-**1**

been reported.[7] However, as with schizozygine, no AC for any schizozygane alkaloid has been established. The AC of schizozygine cannot be inferred, therefore, from the AC of another member of the group.

Remarkably, an alkaloid very closely related to schizozygine, strempeliopine, was isolated from the Cuban plant *Strempeliopsis strempelioides* and shown to have the structure **2**,[8−11] differing from schizozygine only in the absence of ring F and the hydrogenation of the C14−C15 double bond.

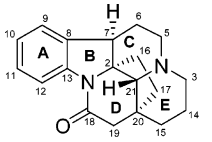

(2S,7R,20R,21R)-(-)-**2**

The AC of (−)-**2** was shown to be 2*S*,7*R*,20*R*,21*R* by Hájíček and Trojánek[9] via stereospecific synthesis from 18-methylenevincadifformine, whose AC was established by comparison of its electronic circular dichroism (ECD) spectrum to the ECD spectra of vincadifformine and tabersonine, indole alkaloids of known AC.[12] The specific rotation $[\alpha]_{578}$ of strempeliopine is −25.4 (MeOH),[9] opposite in sign to the $[\alpha]_D$ of schizozygine. Given the similarity in structure of **1** and **2**, one might conclude from their oppositely signed specific rotations that the AC of (+)-schizozygine is 2*R*,7*S*,20*S*,21*S*. However, this conclusion could not be relied upon since optical rotation can be very sensitive to small changes in structure. For example, the N-methylation of andrangine, which does not change the AC, changes $[\alpha]_D$ from −42 to +60.5.[13] In addition, even though their structures are so similar, since schizozygine and strempeliopine are obtained from different plant species it cannot be safely assumed that the biosynthetic pathways to these molecules, and hence their ACs, are identical.

The ACs of other indole alkaloids from other plant species, for example, vallesamidine,[14] andrangine,[13] and aspidospermidine,[15,16] have been determined.[17] As with strempeliopine, these ACs cannot be transferred to schizozygine.

Here, we report direct determination of the AC of schizozygine from its vibrational circular dichroism (VCD) spectrum, its electronic circular dichroism (ECD) spectrum, and its optical rotation (OR). For each chiroptical property, the AC is deduced by comparison of the experimental data to density functional theory (DFT) calculations for the two enantiomers. The application of DFT to the prediction of VCD spectra began in the early 1990s[18] and culminated in 1996 in the full DFT implementation of Stephens' equation for vibrational rotational strengths[19] by Cheeseman et al.[18f] Since 1998 this latter methodology has been commercially available via the GAUSSIAN program,[20] leading to extensive usage of VCD spectroscopy in determining ACs.[21] The time-dependent density functional theory (TDDFT) methodology was subsequently applied to the prediction of ECD spectra[22] and of transparent spectral region OR,[22,23] and since 2003 these methodologies have been simultaneously available in the GAUSSIAN program, making the use of the ECD and OR phenomena for determining ACs more reliable than heretofore. While ACs can be determined using only a single chiroptical property, the concerted use of all three properties clearly provides more definitive ACs. The first concerted application of the DFT calculation of VCD, ECD, and OR to the determination of the AC of a natural product was recently reported for the sesquiterpene natural product

(8) Hájíček, J.; Trojánek, J. *Tetrahedron Lett.* **1981**, *22*, 2927−2928.
(9) Hájíček, J.; Trojánek, J. *Tetrahedron Lett.* **1982**, *23*, 365−368.
(10) Laguna, A.; Novotny, L.; Dolejs, L.; Budesinsky, M. *Planta Med.* **1984**, *50*, 285−288.
(11) Hájíček, J.; Trojánek, J. *Collect. Czech. Chem. Commun.* **1986**, *51*, 1731−1742.
(12) Klyne, W.; Buckingham, J. *Atlas of stereochemistry: absolute configurations of organic molecules*; Oxford University Press: New York, 1974; p 152.
(13) Kan-Fan, C.; Das, B. C.; Husson, H. P.; Potier, P. *Bull. Soc. Chim. Fr.* **1974**, 2839−2841.
(14) Brown, S. H.; Djerassi, C.; Simpson, P. G. *J. Am. Chem. Soc.* **1968**, *90*, 2445−2446.
(15) Klyne, W.; Swan, R. J.; Bycroft, B. W.; Schumann, D.; Schmid, H. *Helv. Chim. Acta* **1965**, *48*, 443−452.
(16) Camerman, A.; Camerman, N.; Kutney, J. P.; Piers, E.; Trotter, J. *Tetrahedron Lett.* **1965**, *6*, 637−642.
(17) Klyne, W.; Buckingham, J. *Atlas of stereochemistry: absolute configurations of organic molecules*; Oxford University Press: New York, 1974.
(18) (a) Stephens, P. J.; Devlin, F. J.; Chabalowski, C. F.; Frisch, M. J. *J. Phys. Chem.* **1994**, *98*, 11623−11627. (b) Stephens, P. J.; Devlin, F. J.; Ashvar, C. S.; Chabalowski, C. F.; Frisch, M. J. *Faraday Discuss.* **1994**, *99*, 103−119. (c) Bak, K. L.; Devlin, F. J.; Ashvar, C. S.; Taylor, P. R.; Frisch, M. J.; Stephens, P. J. *J. Phys. Chem.* **1995**, *99*, 14918−14922. (d) Devlin, F. J.; Finley, J. W.; Stephens, P. J.; Frisch, M. J. *J. Phys. Chem.* **1995**, *99*, 16883−16902. (e) Stephens, P. J.; Devlin, F. J.; Ashvar, C. S.; Bak, K. L.; Taylor, P. R.; Frisch, M. J. In *Chemical Applications of Density-Functional Theory*; Laird, B. B., Ross, R. B., Ziegler, T., Eds.; ACS Symposium Series, Vol. 629; American Chemical Society: Washington, DC, 1996; pp 105−113. (f) Cheeseman, J. R.; Frisch, M. J.; Devlin, F. J.; Stephens, P. J. *Chem. Phys. Lett.* **1996**, *252*, 211−220.
(19) Stephens, P. J. *J. Phys. Chem.* **1985**, *89*, 748−752.
(20) GAUSSIAN, Gaussian, Inc., www.gaussian.com.
(21) See, for example: (a) Ashvar, C. S.; Stephens, P. J.; Eggimann, T.; Wieser, H. *Tetrahedron: Asymmetry* **1998**, *9*, 1107−1110. (b) Aamouche, A.; Devlin, F. J.; Stephens, P. J. *Chem. Commun.* **1999**, 361−362. (c) Stephens, P. J.; Devlin, F. J. *Chirality* **2000**, *12*, 172−179. (d) Aamouche, A.; Devlin, F. J.; Stephens, P. J. *J. Am. Chem. Soc.* **2000**, *122*, 2346−2354. (e) Aamouche, A.; Devlin, F. J.; Stephens, P. J.; Drabowicz, J.; Bujnicki, B.; Mikolajczyk, M. *Chem.—Eur. J.* **2000**, *6*, 4479−4486. (f) Stephens, P. J.; Aamouche, A.; Devlin, F. J.; Superchi, S.; Donnoli, M. I.; Rosini, C. *J. Org. Chem.* **2001**, *66*, 3671−3677. (g) Devlin, F. J.; Stephens, P. J.; Scafato, P.; Superchi, S.; Rosini, C. *Tetrahedron: Asymmetry* **2001**, *12*, 1551−1558. (h) Stephens, P. J.; Devlin, F. J.; and Aamouche, A. In *Chirality: Physical Chemistry*; Hicks, J. M., Ed.; ACS Symposium Series, Vol. 810; American Chemical Society: Washington, DC, 2002; Chapt. 2, pp 18−33. (i) Devlin, F. J.; Stephens, P. J.; Scafato, P.; Superchi, S.; Rosini, C. *Chirality* **2002**, *14*, 400−406. (j) Devlin, F. J.; Stephens, P. J.; Oesterle, C.; Wiberg, K. B.; Cheeseman, J. R.; Frisch, M. J. *J. Org. Chem.* **2002**, *67*, 8090−8096. (k) Stephens, P. J. In *Computational Medicinal Chemistry for Drug Discovery*; Bultinck, P., de Winter, H., Langenaecker, W., Tollenaere, J., Eds.; Dekker: New York, 2003; Chapt. 26, pp 699−725. (l) Cere, V.; Peri, F.; Pollicino, S.; Ricci, A.; Devlin, F. J.; Stephens, P. J.; Gasparrini, F.; Rompietti, R.; Villani, C. *J. Org. Chem.* **2005**, *70*, 664−669. (m) Stephens, P. J.; McCann, D. M.; Devlin, F. J.; Flood, T. C.; Butkus, E.; Stoncius, S.; Cheeseman, J. R. *J. Org. Chem.* **2005**, *70*, 3903−3913. (n) Devlin, F. J.; Stephens, P. J.; Besse, P. *Tetrahedron: Asymmetry* **2005**, *16*, 1557−1566. (o) Devlin, F. J.; Stephens, P. J.; Bortolini, O. *Tetrahedron: Asymmetry* **2005**, *16*, 2653−2663. (p) Carosati, E.; Cruciani, G.; Chiarini, A.; Budriesi, R.; Ioan, P.; Spisani, R.; Spinelli, D.; Cosimelli, B.; Fusi, F.; Frosini, M.; Matucci, R.; Gasparrini, F.; Ciogli, A.; Stephens, P. J.; Devlin, F. J. *J. Med. Chem.* **2006**, *49*, 5206−5216.
(22) (a) Stephens, P. J.; McCann, D. M.; Butkus, E.; Stoncius, S.; Cheeseman, J. R.; Frisch, M. J. *J. Org. Chem.* **2004**, *69*, 1948−1958. (b) Stephens, P. J.; McCann, D. M.; Devlin, F. J.; Cheeseman, J. R.; Frisch, M. J. *J. Am. Chem. Soc.* **2004**, *126*, 7514−7521. (c) McCann, D. M.; Stephens, P. J. *J. Org. Chem.* **2006**, *71*, 6074−6098.

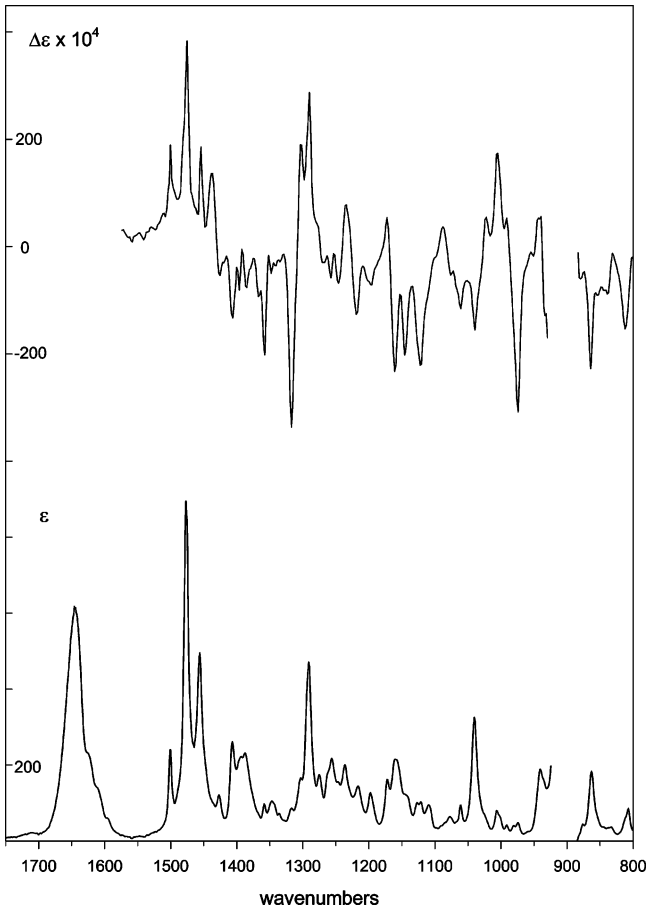


**FIGURE 2.** Experimental IR and VCD spectra of (+)-**1**.

quadrone.[24] Here, we extend this work to the case of schizozygine. The AC of (+)-schizozygine is unambiguously shown to be 2*R*,7*S*,20*S*,21*S*. With the assumption that schizogamine and schizogaline share a common biosynthetic pathway with schizozygine, this finding simultaneously also establishes their ACs.

## Experimental Section

**Spectroscopy.** IR and VCD spectra of $CDCl_3$ solutions of (+)-**1** were obtained using a Thermo-Nicolet Nexus 670 IR spectrometer and a Bomem/BioTools Chiral/IR VCD spectrometer at resolutions of 1 and 4 $cm^{-1}$ respectively. The VCD instrument is equipped with a dual photo-elastic modulator accessory, in order to reduce VCD artifacts, a methodology invented and implemented by Dr. J. C. Cheng at the University of Southern California in 1975.[25] All measurements used an International Crystal Laboratories (ICL) SL-3 cell with KBr windows, 99.4 $\mu$m path length, and a sample volume of ~50 $\mu$L. VCD scans were 1 h.

ECD spectra were measured using a Jasco J-810 spectropolarimeter and a 0.01 cm quartz cell. Resolution 1 nm, time constant 1 s, scan speed 100 nm/min, and 10 accumulations were used. Baselines were the spectra of the solvent obtained under the same conditions.

Optical rotations of $CHCl_3$ and $CDCl_3$ solutions of (+)-**1** were measured on Perkin-Elmer 141 and 241 polarimeters.

**Calculations.** Calculations have been carried out on (2*R*,7*S*,20*S*,21*S*)-**1** and (2*R*,7*S*,20*S*,21*S*)-**2**. Initial conformational analyses were carried out using Monte Carlo searching together with the MMFF94 molecular mechanics force field via the SPARTAN 02 program.[26] Geometry optimizations of the MMFF94 conformations obtained were then carried out by DFT via the GAUSSIAN 03 program,[20] followed by calculations of their harmonic vibrational frequencies to verify their stability and to calculate conformational free energies. Starting from the DFT conformations obtained, further conformational analysis was subsequently carried out using DFT potential energy surface (PES) scans, followed by optimizations of additional PES minima identified and harmonic vibrational frequency calculations. Simultaneously with vibrational frequency calculations, harmonic vibrational dipole strengths and rotational strengths were calculated and IR and VCD spectra were obtained thence, using Lorentzian band shapes.[27] The DFT calculation of vibrational rotational strengths in GAUSSIAN 03 uses the equation of Stephens[19] and its DFT implementation by Cheeseman et al. with gauge-invariant atomic orbitals (GIAOs), which guarantee origin-independent rotational strengths.[18f]

Experimental vibrational frequencies, dipole strengths, and rotational strengths were obtained from experimental IR and VCD spectra by Lorentzian fitting[27] using the PeakFit program.[28]

Electronic excitation energies, oscillator strengths, and rotational strengths of the DFT conformations of **1** have been calculated using TDDFT via GAUSSIAN 03, and ECD spectra obtained thence using Gaussian band shapes.[22c]

Optical rotations of the DFT conformations of **1** and **2** have been calculated using TDDFT via GAUSSIAN 03.

As in prior work,[21−23] DFT calculations have used the functionals B3LYP and B3PW91 and the basis sets 6-31G* and TZ2P for IR and VCD calculations and B3LYP and aug-cc-pVDZ for ECD and OR calculations.

## Results

**Isolation of Schizozygine.** Leaves of *Schizozygia caffaeoides* (Boj.) Baill. were collected in July 1996 on the seaside of the Mombasa region, Kenya, by Sedaherb S.A. (Saint Léger sur Dheume, France).

Dried material was grained and macerated repeatedly with methanol. The macerate was processed by acido-basic treatment, and then by repeated chromatography on alumina and silica gel as described elsewhere.[29] Crude (+)-schizozygine was recrystallized from methanol, mp 191.5−194.5 °C (decomp), $[\alpha]_D^{23}$ +18.1 (*c* 0.63; $CHCl_3$), lit.[1] mp 192−194 °C, $[\alpha]_D^{23}$ +15.5 (*c* 1; $CHCl_3$).

**Conformational Analysis.** A Monte Carlo conformational search using the MMFF94 molecular mechanics force field, with a 20 kcal/mol window, found only two conformations of **1**, **a** and **b**, **a** being lower in energy than **b**; their relative energies are given in Table 1. Conformations **a** and **b** differ principally with regard to the conformation of ring C. In **a** and **b** ring C is in boat and chair conformations, respectively. The geometries

(23) (a) Stephens, P. J.; Devlin, F. J.; Cheeseman, J. R.; Frisch, M. J.; Mennucci, B.; Tomasi, J. *Tetrahedron: Asymmetry* **2000**, *11*, 2443−2448. (b) Stephens, P. J.; Devlin, F. J.; Cheeseman, J. R.; Frisch, M. J. *J. Phys. Chem. A* **2001**, *105*, 5356−5371. (c) Stephens, P. J.; Devlin, F. J.; Cheeseman, J. R.; Frisch, M. J. *Chirality* **2002**, *14*, 288−296. (d) Stephens, P. J.; Devlin, F. J.; Cheeseman, J. R.; Frisch, M. J.; Rosini, C. *Org. Lett.* **2002**, *4*, 4595−4598. (e) Stephens, P. J.; Devlin, F. J.; Cheeseman, J. R.; Frisch, M. J.; Bortolini, O.; Besse, P. *Chirality* **2003**, *15*, S57−S64. (f) McCann, D. M.; Stephens, P. J.; Cheeseman, J. R. *J. Org. Chem.* **2004**, *69*, 8709−8717.

(24) Stephens, P. J.; McCann, D. M.; Devlin, F. J.; Smith, A. B., III *J. Nat. Prod.* **2006**, *69*, 1055−1064.

(25) Cheng, J. C.; Nafie, L. A.; Stephens, P. J. *J. Opt. Soc. Am.* **1975**, *65*, 1031−1035.

(26) Spartan 02; Wavefunction, Inc., www.wavefun.com.

(27) (a) Devlin, F. J.; Stephens, P. J.; Cheeseman, J. R.; Frisch, M. J. *J. Phys. Chem. A* **1997**, *101*, 6322−6333. (b) Devlin, F. J.; Stephens, P. J.; Cheeseman, J. R.; Frisch, M. J. *J. Phys. Chem. A* **1997**, *101*, 9912−9924.

(28) PeakFit, 4th ed.; Jandel Scientific Software: 1995.

(29) Hajicek, J.; Budesinsky, M. Manuscript in preparation.

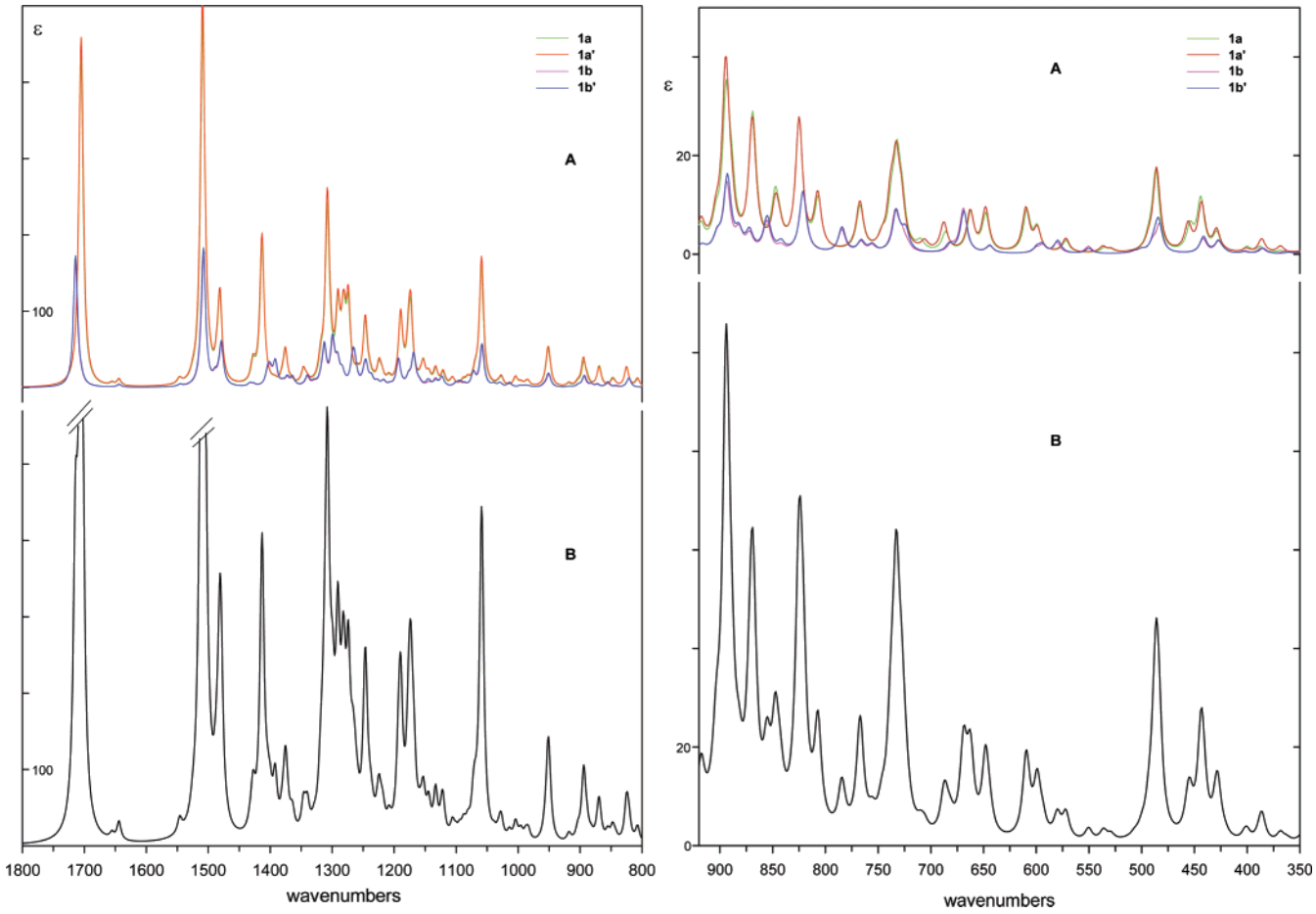


**FIGURE 3.** (a) B3LYP/TZ2P IR spectra of **1** for the range 800−1800 $cm^{-1}$: (A) Population-weighted spectra of the four conformations; (B) the conformationally averaged spectrum. (b) B3LYP/TZ2P IR spectra of **1** for the range 350−920 $cm^{-1}$: (A) the population-weighted spectra of the four conformations; (B) the conformationally averaged spectrum. Band shapes are Lorentzian; $\gamma = 4.0$ $cm^{-1}$.

of conformations **1a** and **1b** were then reoptimized at the B3LYP/6-31G* level. Their relative energies are given in Table 1. While conformation **1b** remains higher in energy than **1a**, the B3LYP/6-31G* energy difference is much smaller than the MMFF94 value. Calculation of the B3LYP/6-31G* harmonic vibrational frequencies of **1a** and **1b** confirmed that they are stable conformations and led to the relative free energies, also given in Table 1.

In contrast to the MMFF94 structures of **1a** and **1b**, where ring F is very close to planar, in the B3LYP/6-31G* structures of **1a** and **1b** ring F is substantially puckered, and, surprisingly, oppositely puckered in the two conformations. We therefore carried out a potential energy surface (PES) scan at the B3LYP/6-31G* level, varying the dihedral angle C9−C10−O−C24 for both conformations **1a** and **1b**. The results, shown in Figure 1 of the Supporting Information, clearly demonstrate the existence of an additional conformation of ring F for each conformation of ring C. Optimization led to the new conformations **1a′** and **1b′** with the relative energies given in Table 1. Frequency calculations proved their stability and led to the relative free energies given in Table 1. Conformation **1a′** has the same conformation of ring C as **1a** and is very similar in energy. Likewise, conformation **1b′** has the same conformation of ring C as **1b** and is almost identical in energy.

To confirm that no other conformations of **1** exist, we have also scanned the PES at the B3LYP/6-31G* level, varying the dihedral angles C2−C21−C20−C19, C21−C2−C7−C6, C2−C21−N−C5, and C20−C21−N−C3, for conformations **1a** and **1b**. The results are shown in Figures 2−5 of the Supporting Information; no additional conformations were found.

The geometries of the four conformations of **1** were further reoptimized at the B3LYP/TZ2P and B3PW91/TZ2P levels, and vibrational frequencies calculated. The resulting relative energies and free energies are given in Table 1, together with the equilibrium room-temperature populations calculated from the relative free energies. At all levels, the percentage populations of conformations **1a** and **1a′** are 35−40% and the populations of conformations **1b** and **1b′** are 10−15%. At least 70% of the equilibrium mixture is thus predicted to be conformations **1a** and **1a′**.

The "heavy-atom" dihedral angles of the MMFF94, B3LYP/6-31G*, B3LYP/TZ2P, and B3PW91/TZ2P structures of the four conformations of **1** are given in Table 1 of the Supporting Information. The B3PW91/TZ2P structures are shown in Figure 1. In all DFT geometries ring F is puckered, the direction of puckering being the same in conformations **1a** and **1b′** and in **1a′** and **1b** and opposite in **1a** and **1a′** and in **1b** and **1b′**. Ring A is essentially planar in all geometries. Ring B is slightly puckered, similarly in **1a** and **1a′**, and in **1b** and **1b′**. Ring C is substantially nonplanar, with similar boat conformations in **1a** and **1a′** and chair conformations in **1b** and **1b′**, corresponding to different relative positions of C6. Rings D and E and the five-membered ring C2−C16−C17−C20−C21 are each nonplanar, with similar geometries in all four conformations.

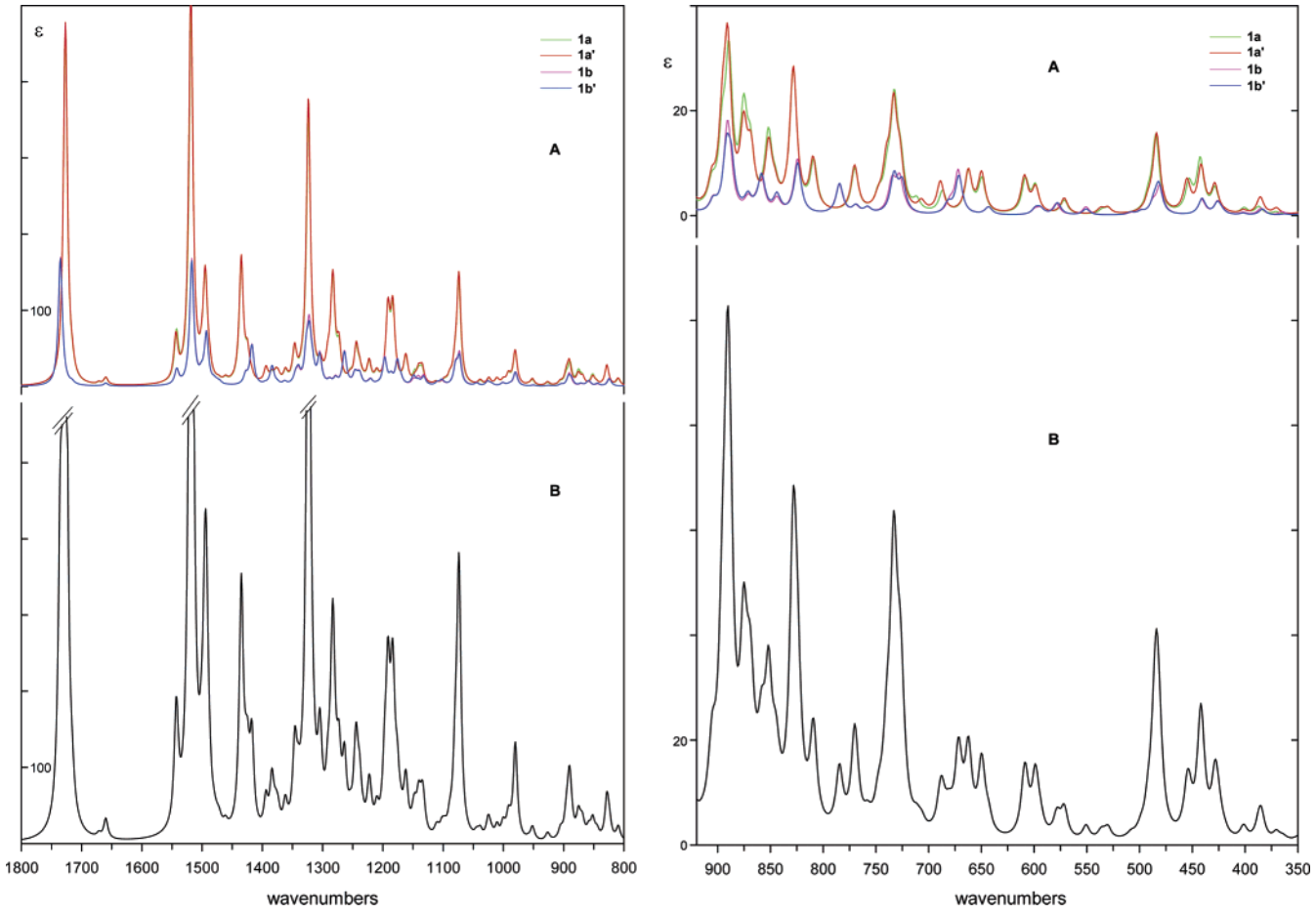


**FIGURE 4.** (a) B3PW91/TZ2P IR spectra of **1** for the range 800−1800 $cm^{-1}$: (A) population-weighted spectra of the four conformations; (B) the conformationally averaged spectrum. (b) B3PW91/TZ2P IR spectra of **1** for the range 350−920 $cm^{-1}$: (A) the population-weighted spectra of the four conformations; (B) the conformationally averaged spectrum. Band shapes are Lorentzian; $\gamma = 4.0$ $cm^{-1}$.

In Figures 6 and 7 of the Supporting Information, the B3PW91/TZ2P "heavy-atom" dihedral angles of the pairs of conformations **1a** and **1a′**, **1b** and **1b′**, **1a** and **1b′**, and **1b** and **1a′** are compared. The close similarity in structures of **1a** and **1a′** and of **1b** and **1b′**, with the exception of ring F, are clearly seen in Figure 6 of the Supporting Information. The much greater differences between structures **1a** and **1b′** and structures **1b** and **1a′**, especially for ring C, are clearly seen in Figure 7 of the Supporting Information.

**IR and VCD Spectra.** The IR and VCD spectra of (+)-**1** have been measured in $CDCl_3$ solution at concentrations of 0.127, 0.253, and 0.425 M with a cell of path length 99.4 $\mu$m. The baseline for the IR spectrum was the IR spectrum of $CDCl_3$. In the absence of racemic **1**, the baseline for the VCD spectrum of (+)-**1** was the VCD spectrum of $CDCl_3$. The IR spectra, in units of $A$ and $\epsilon$, are shown in Figures 8 and 9 of the Supporting Information over the range 350−1800 $cm^{-1}$. The VCD spectra, in units of $\Delta A$ and $\Delta\epsilon$, are shown in Figure 10 of the Supporting Information over the range 800−1800 $cm^{-1}$. The IR spectra in $\epsilon$ units are superposable, demonstrating the concentration-independence of the IR spectrum over the range 0.1−0.5 M. The VCD spectra in $\Delta\epsilon$ units are not perfectly superposable. The variations are attributable to artifacts generated by the Bomem/BioTools VCD instrument, despite the incorporation of the dual-PEM accessory. As seen in Figure 10 of the Supporting Information, artifacts are much greater in the carbonyl stretching region at >1600 $cm^{-1}$. In order to reduce absorbance-related artifacts, we have deleted sections of the VCD spectra for which $A$ values are >1.0, with the results shown in Figure 11 of the Supporting Information. The remaining differences in the three VCD spectra provide a gauge of the artifact levels that remain at $A$ values ≤ 1.0. Without a racemic sample, or the second enantiomer, these artifacts cannot be removed by subtraction, and they remain as uncertainties in our VCD spectra. Finally, a composite VCD spectrum is arrived at by combining sections of the VCD spectra of the three solutions with the criteria that for each section (1) corresponding $A$ values are ≤1.0 and (2) the concentration, and therefore $\Delta A$ and the signal-to-noise ratio, are maximal. The resulting VCD spectrum is also shown in Figure 11 of the Supporting Information. Because of the poor reproducibility of the VCD spectrum at > 1600 $cm^{-1}$, this region is excluded from the composite spectrum. The final VCD spectrum of (+)-**1** is shown, together with the IR spectrum, in Figure 2.

The harmonic frequencies and dipole strengths of all four conformations of **1** have been calculated using DFT at the B3LYP/TZ2P and B3PW91/TZ2P levels, with the results given in Table 2 of the Supporting Information. The IR spectra obtained thence using Lorentzian band shapes are shown in Figures 12 and 13 of the Supporting Information for the frequency range 800−1800 $cm^{-1}$. For both functionals, the spectra of **1a** and **1a′** are extremely similar, as are the spectra

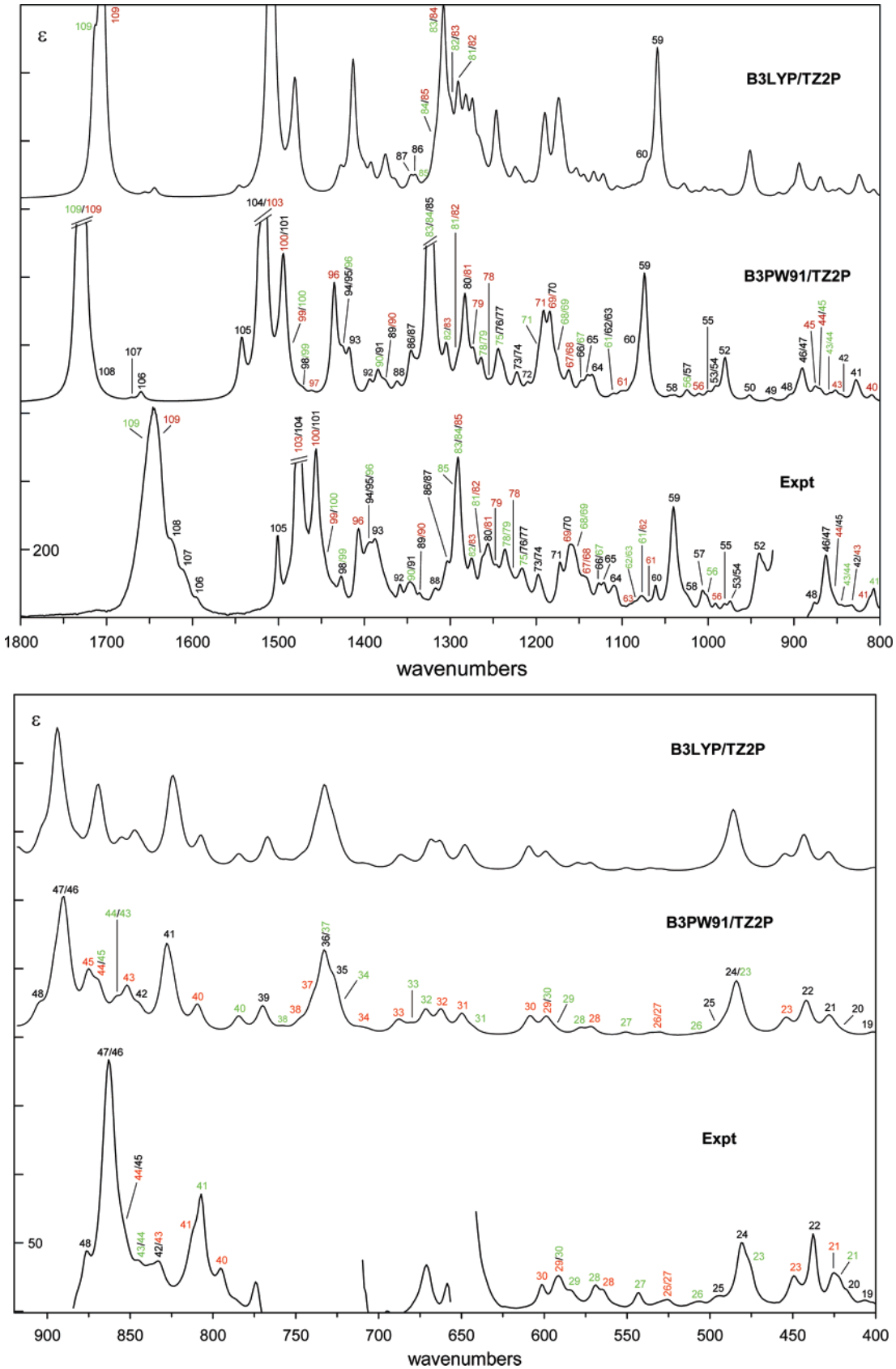


**FIGURE 5.** Comparison of experimental and conformationally averaged B3LYP/TZ2P and B3PW91/TZ2P IR spectra of **1** for the range 800−1800 $cm^{-1}$ (a) and for the range 400−920 $cm^{-1}$ (b). Fundamentals are numbered. The experimental assignment is based on the B3PW91/TZ2P spectrum. Red and green numbers indicate bands of **1a**/**1a′** and **1b**/**1b′**, respectively. Black numbers indicate superpositions of bands **1a**, **1a′**, **1b**, and **1b′**.

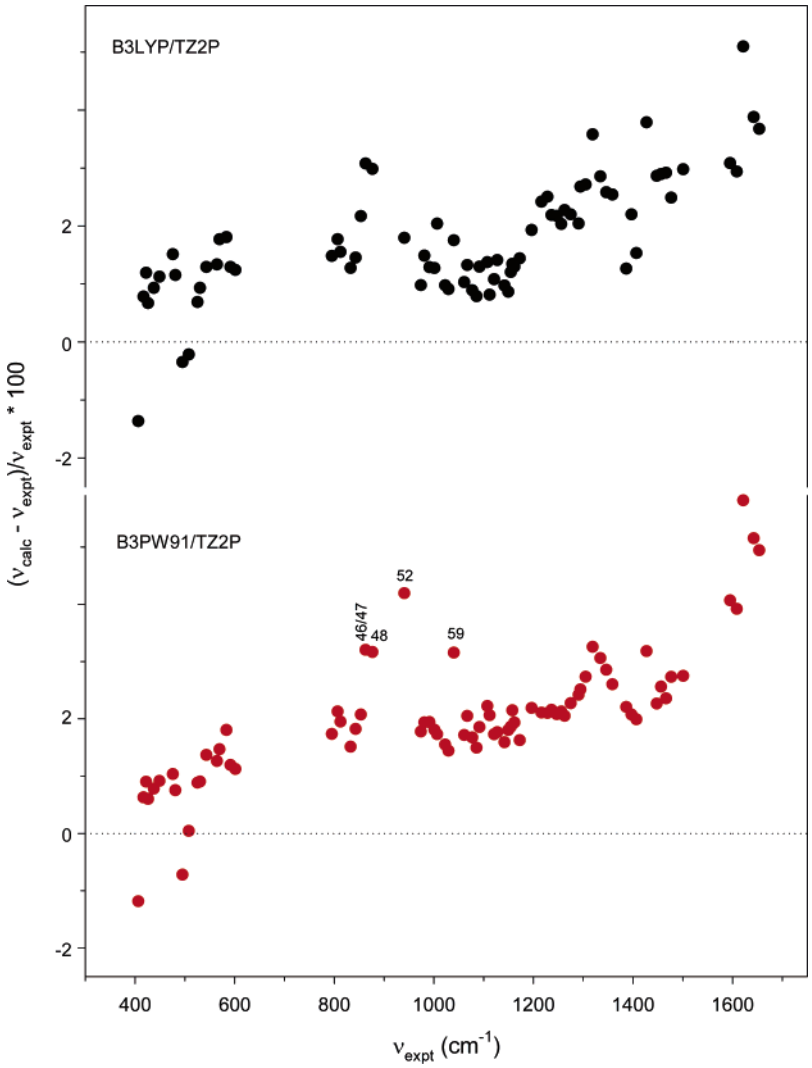


**FIGURE 6.** Comparison of calculated and experimental frequencies of **1**. The numbers are fundamentals.

of **1b** and **1b′**. The spectra of **1a** and **1b**, in contrast, differ significantly. These results show that the IR spectrum of **1** is sensitive to the conformation of ring C but very insensitive to the conformation of ring F. The IR spectrum of the equilibrium mixture of conformations **1a**, **1a′**, **1b**, and **1b′** is given by:

$$\epsilon(\nu) = \sum_{i=1}^{4} x_i \epsilon_i(\nu)$$

where $x_i$ and $\epsilon_i$ are the mole fraction and IR spectrum of the *i*th conformation. The population-weighted spectra of the four conformations of **1** are shown in Figures 3 and 4 together with their sum, the predicted spectrum of the conformational mixture of **1**, for the frequency range 350−1800 cm$^{-1}$. The conformationally averaged B3LYP/TZ2P and B3PW91/TZ2P spectra are compared to each other and to the experimental IR spectrum in Figure 5. The B3PW91/TZ2P and B3LYP/TZ2P spectra are similar but not identical. The B3PW91/TZ2P spectrum is in better agreement with the experimental spectrum. Accordingly, we base our assignment of the experimental spectrum on the B3PW91/TZ2P spectrum. The assignment which results is shown in detail in Figure 5.

Overall, the agreement between the B3PW91/TZ2P spectrum and the experimental spectrum is very good, allowing for the shift to higher frequency of the calculated spectrum due to the absence of anharmonicity,[30] providing strong support for the reliability of the B3PW91/TZ2P conformational structures and relative free energies. The most intense features of the experimental spectrum are perfectly reproduced by the calculated spectrum; for example, the experimental bands at 438, 481, 807, 863, 1040, 1291, 1456, 1477 and 1645 which are unambiguously assignable to modes 22 of **1a/1a′/1b/1b′**, 24 of **1a/1a′/1b/1b′**, 41 of **1b/1b′**, 46 and 47 of **1a/1a′/1b/1b′**, 59 of **1a/1a′/1b/1b′**, 83 of **1b/1b′** and 84 of **1b/1b′** and 85 of **1a/1a′**, 100 of **1a/1a′** and 101 of **1a/1a′/1b/1b′**, 103 of **1a/1a′**, and 104 of **1a/1a′/1b/1b′**, and 109 of **1a/1a′/1b/1b′** respectively. In addition, there is plentiful evidence of the experimental existence of the two pairs of conformers, **1a**/ **1a′** and **1b**/**1b′**. Modes 21, 23, 26/27, 28, 30, 40, 41, 56, 67/68, and 96 of **1a**/**1a′** and modes 21, 23, 26−29, 41, 43/44, 56, and 78/79 of **1b**/**1b′** are clearly resolved and assignable in the experimental spectrum.

In order to compare calculated and experimental frequencies and dipole strengths quantitatively, we have carried out a Lorentzian fitting[27] of the experimental IR spectrum (0.425 M), with the results given in Table 2 and Figure 14 of the Supporting

(30) Finley, J. W.; Stephens, P. J. *J. Mol. Struct. (THEOCHEM)* **1995**, *357*, 225−235.

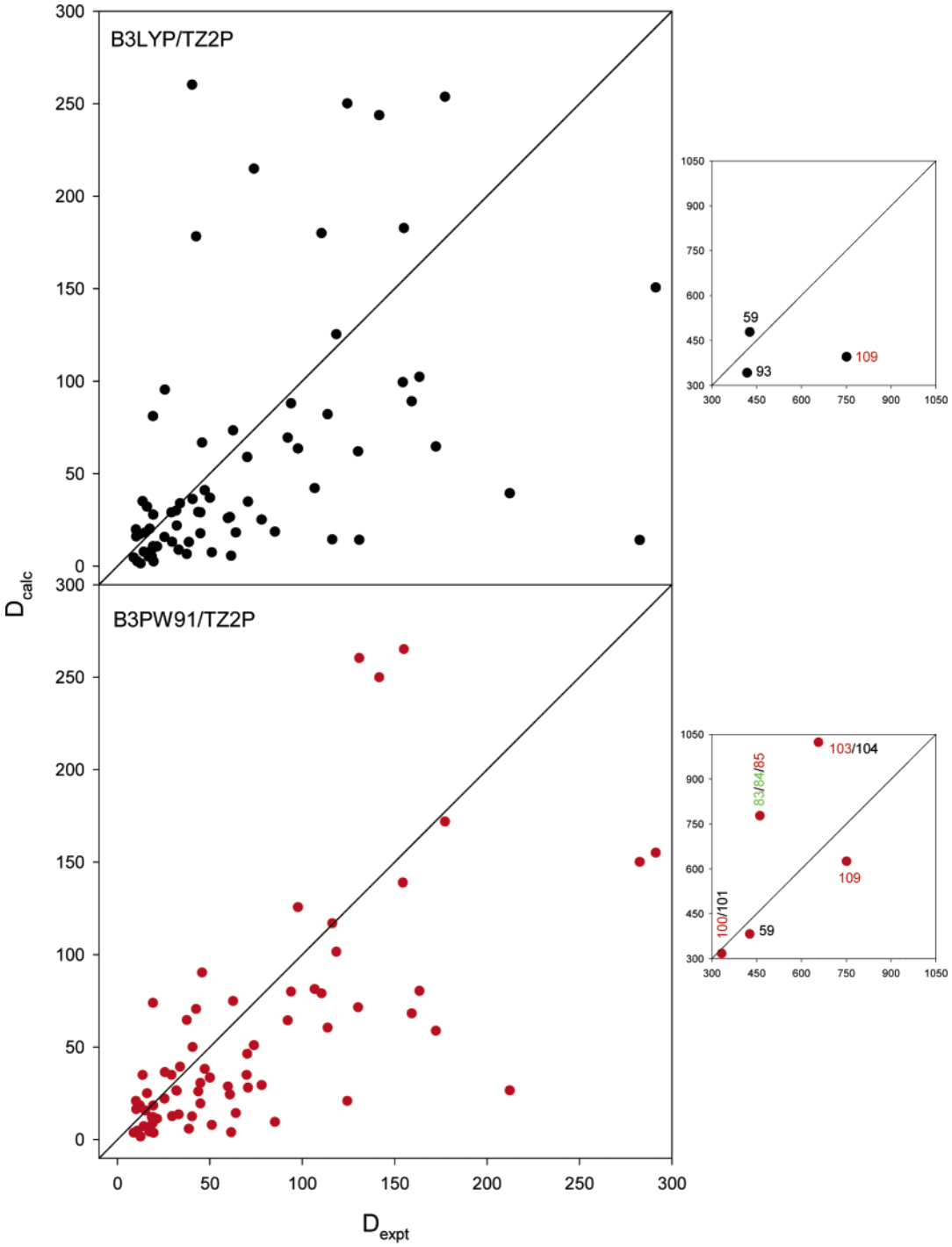


**FIGURE 7.** Comparison of calculated and experimental dipole strengths of **1**. Calculated dipole strengths are population-weighted averages. Dipole strengths greater than 300 are shown in the insets. The lines are of +1 slope. Dipole strengths are in units of $10^{-40}$ esu$^2$ cm$^2$. The numbers are fundamentals (color code as in Figure 5).

Information. Calculated and experimental frequencies and dipole strengths are compared in Figures 6 and 7 respectively.

The rotational strengths of all four conformations of (2*R*,7*S*,-20*S*,21*S*)-**1** have been calculated using DFT at the B3LYP/TZ2P and B3PW91/TZ2P levels, with the results given in Table 2 of the Supporting Information. The VCD spectra obtained thence by use of Lorentzian band shapes are shown in Figures 15 and 16 of the Supporting Information. For both functionals, the spectra of **1a** and **1a′** are similar but differ much more than do their IR spectra. The same situation obtains for the spectra of **1b** and **1b′**. The VCD spectra of **1a**/**1a′** and **1b**/**1b′** differ much more dramatically than do their IR spectra. These results show that the VCD spectrum of **1** is more sensitive to the conformations of both rings C and F than is the IR spectrum. The VCD spectrum of the equilibrium mixture of conformations **1a**, **1a′**,

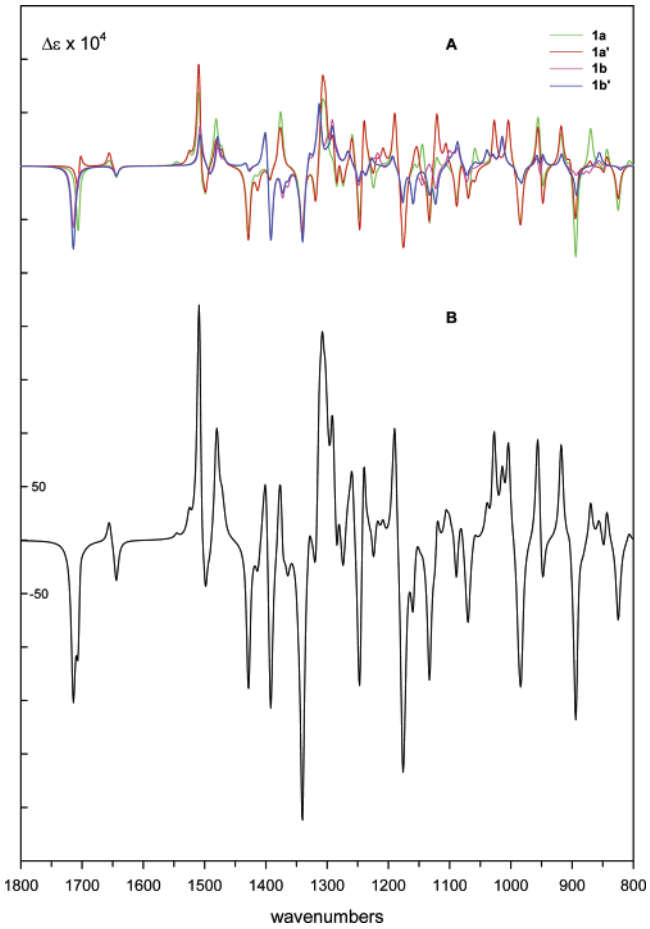


**FIGURE 8.** B3LYP/TZ2P VCD spectra of (2*R*,7*S*,20*S*,21*S*)-**1**: (A) population-weighted spectra of the four conformations; (B) the conformationally averaged spectrum. Band shapes are Lorentzian; $\gamma$ = 4.0 cm$^{-1}$.

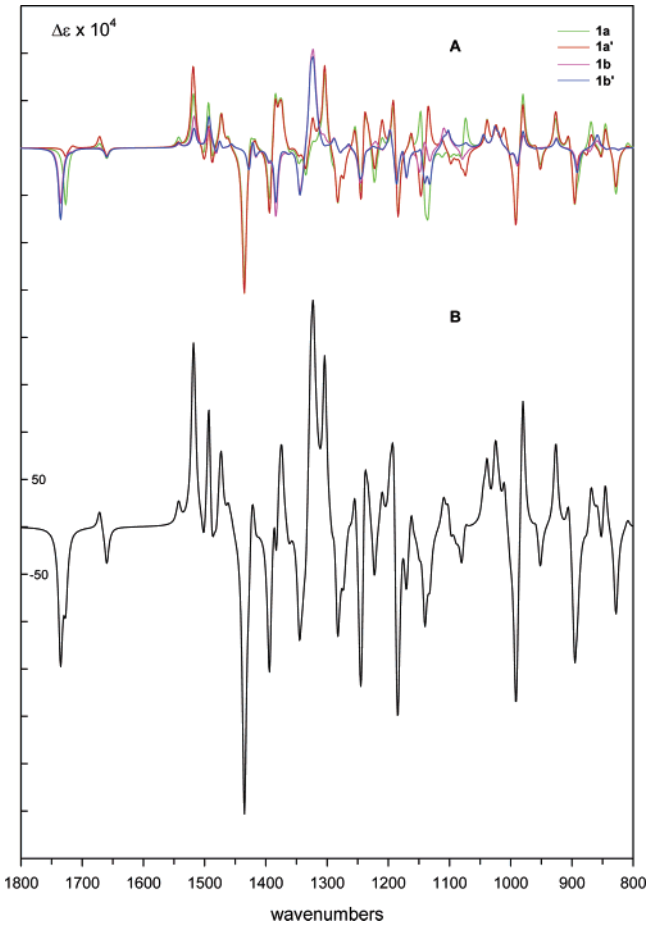


**FIGURE 9.** B3PW91/TZ2P VCD spectra of (2*R*,7*S*,20*S*,21*S*)-**1**: (A) population-weighted spectra of the four conformations; (B) the conformationally averaged spectrum. Band shapes are Lorentzian; $\gamma$ = 4.0 cm$^{-1}$.

**1b**, and **1b′** is given by

$$\Delta\epsilon(\nu) = \sum_{i=1}^{4} x_i \Delta\epsilon_i(\nu)$$

where $x_i$ and $\Delta\epsilon_i$ are the mole fraction and VCD spectrum of the *i*th conformation. The population-weighted VCD spectra of the four conformations of **1** are shown in Figures 8 and 9 together with the conformationally averaged spectra. The B3LYP/TZ2P and B3PW91/TZ2P conformationally averaged spectra are compared to each other and to the experimental VCD spectrum of (+)-**1** in Figure 10. As with the IR spectrum, the B3PW91/TZ2P VCD spectrum is in better agreement with the experimental spectrum than the B3LYP/TZ2P spectrum. The assignment of the experimental spectrum that follows from the assignment of the IR spectrum, together with the B3PW91/TZ2P VCD spectrum, is shown in detail in Figure 10.

The B3PW91/TZ2P VCD spectrum of (2*R*,7*S*,20*S*,21*S*)-**1** is in good agreement with the experimental spectrum of (+)-**1** over the range 800−1550 cm$^{-1}$, allowing for the shift to higher frequency of the calculated spectrum due to the absence of anharmonicity, providing further support for the reliability of the B3PW91/TZ2P conformational structures and relative free energies and, most importantly, establishing the AC of **1** as 2*R*,7*S*,20*S*,21*S*−(+). The most intense features of the experimental spectrum are well-reproduced by the calculated spectrum. For example, the experimental bands at 812, 832, 864, 939, 974, 991, 1006, 1023, 1061, 1087, 1121, 1145, 1161, 1172, 1219, 1235, 1358, 1407, 1438, 1454, 1478 and 1500 cm$^{-1}$ are in good agreement with the predicted signs and relative intensities of modes 41 of **1a/1a′**, 42 of **1a/1a′/1b/1b′**, 46 and 47 of **1a/1a′/1b/1b′**, 52 of **1a/1a′/1b/1b′**, 53 and 54 of **1a/1a′/1b/1b′**, 56 of **1a/1a′**, 57 of **1a/1a′/1b/1b′**, 58 of **1a/1a′**, 60 of **1a/1a′/1b/1b′**, 62 and 63 of **1b/1b′**, 65 of **1a/1a′/1b/1b′**, 68 of **1b/1b′**, 70 of **1a/1a′/1b/1b′**, 71 of **1a/1a′/1b/1b′**, 75 of **1b/1b′** and 76 and 77 of **1a/1a′/1b/1b′**, 78 and 79 of **1b/1b′**, 92 of **1a/1a′/1b/1b′**, 96 of **1a/1a′**, 98 of **1a/1a′** and 99 of **1b/1b′**, 100 of **1a/1a′** and 101 of **1a/1a′/1b/1b′**, 103 of **1a/1a′** and 104 of **1a/1a′/1b/1b′**, and 105 of **1a/1a′/1b/1b′**. Agreement is not perfect: the observed negative VCD of the band at 1039 cm$^{-1}$, assigned to modes 59 of **1a/1a′/1b/1b′**, is not correctly predicted; while the observed VCD at 1270−1320 cm$^{-1}$ is qualitatively reproduced, the detailed assignment is different from that arrived at on the basis of the assignment of the corresponding bands in the IR spectrum. It is noteworthy that for modes 82−88, the B3LYP/TZ2P VCD spectrum differs substantially from the B3PW91/TZ2P spectrum, showing that in this region the predicted spectrum is sensitive to the choice of functional. It is likely, therefore, that the less-than-perfect agreement of theory and experiment can be attributed to imperfection of the B3PW91 functional.

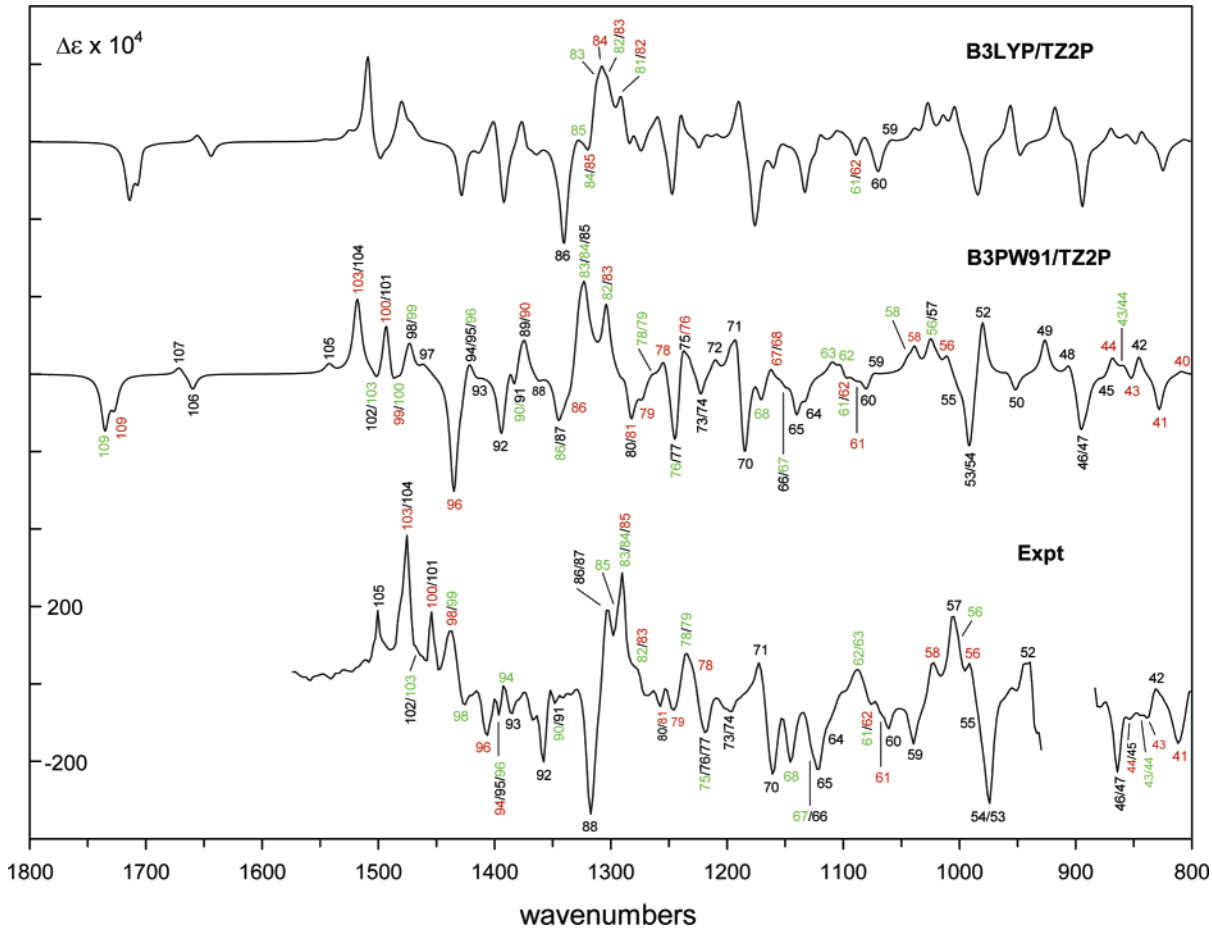


**FIGURE 10.** Comparison of experimental and conformationally averaged B3LYP/TZ2P and B3PW91/TZ2P VCD spectra of **1** for the range 800−1800 $cm^{-1}$. The experimental spectrum is for (+)-**1**. The calculated spectra are for (2*R*,7*S*,20*S*,21*S*)-**1**. Fundamentals are numbered as in Figure 5.

In order to compare calculated and experimental rotational strengths quantitatively we have carried out a Lorentzian fitting of the experimental VCD spectrum with the results given in Table 2 of the Supporting Information and Figure 17 of the Supporting Information. Calculated and experimental rotational strengths are compared in Figure 11. While the quantitative agreement of calculated and experimental rotational strengths is not perfect, as shown in Figure 12, the agreement for the 2*R*,7*S*,20*S*,21*S* AC is far superior to that for the 2*S*,7*R*,20*R*,-21*R* AC. On this basis we unambiguously assign the AC of **1** as (2*R*,7*S*,20*S*,21*S*)-(+).

**UV and ECD Spectra.** The UV and ECD spectra of (+)-**1** have been measured in $CHCl_3$ solution at a concentration of 12.5 mM, using a cell of path length 100 $\mu$m. The baselines were the spectra of $CHCl_3$. The spectra are shown in Figure 13 over the range 220−350 nm.

The B3LYP/aug-cc-pVDZ energies, oscillator strengths, and rotational strengths of the four conformations of (2*R*,7*S*,20*S*,21*S*)-**1** have been calculated at the B3LYP/6-31G*, B3LYP/TZ2P, and B3PW91/TZ2P equilibrium geometries, with the results for the lowest 20 excitations given in Table 3 of the Supporting Information. Rotational strengths were calculated using both length and velocity representations. The small differences between length and velocity rotational strengths confirm that the aug-cc-pVDZ basis set is a good approximation to the basis set limit. The oscillator strengths of the four conformations are plotted in Figure 18 of the Supporting Information. The results for the three geometries are very similar. The excitation energies and oscillator strengths of conformations **1a** and **1a′** are very similar, as are those of **1b** and **1b′**. On the other hand, the excitation energies and oscillator strengths of **1b** and **1b′** differ significantly from those of **1a** and **1a′**. The population-weighted oscillator strengths for the B3PW91/TZ2P geometries are plotted in Figure 14, together with the experimental UV spectrum. The two bands observed experimentally at 315 and 269 nm can be reasonably assigned to excitation 1 of **1a**, **1a′**, **1b**, and **1b′** and excitations 2−4 of **1a**, **1a′**, **1b**, and **1b′** respectively. The origin-independent velocity rotational strengths of the four conformations are plotted in Figures 19−21 of the Supporting Information, together with the ECD spectra obtained thence using Gaussian bandshapes ($\sigma$ = 0.2, 0.3, and 0.4 eV). The results for the three geometries are very similar. As with the UV spectra, the predicted ECD spectra of conformations **1a** and **1a′** are very similar, as are the spectra of conformations **1b** and **1b′**, while the spectra of **1b** and **1b′** differ significantly from those of **1a** and **1a′**. Population-weighted spectra and the conformationally averaged ECD spectra are compared to the experimental spectrum in Figures 22−24 of the Supporting Information. The conformationally averaged ECD spectra of (2*R*,7*S*,20*S*,21*S*)-**1**, based on the B3PW91/TZ2P geometries, are compared to the experimental spectrum in Figure 15. The conformationally averaged spectra for (2*R*,7*S*,20*S*,21*S*)-**1** at all three $\sigma$ values exhibit three principal features at wavelengths ~300, ~270, and ~240 nm with positive, negative, and positive

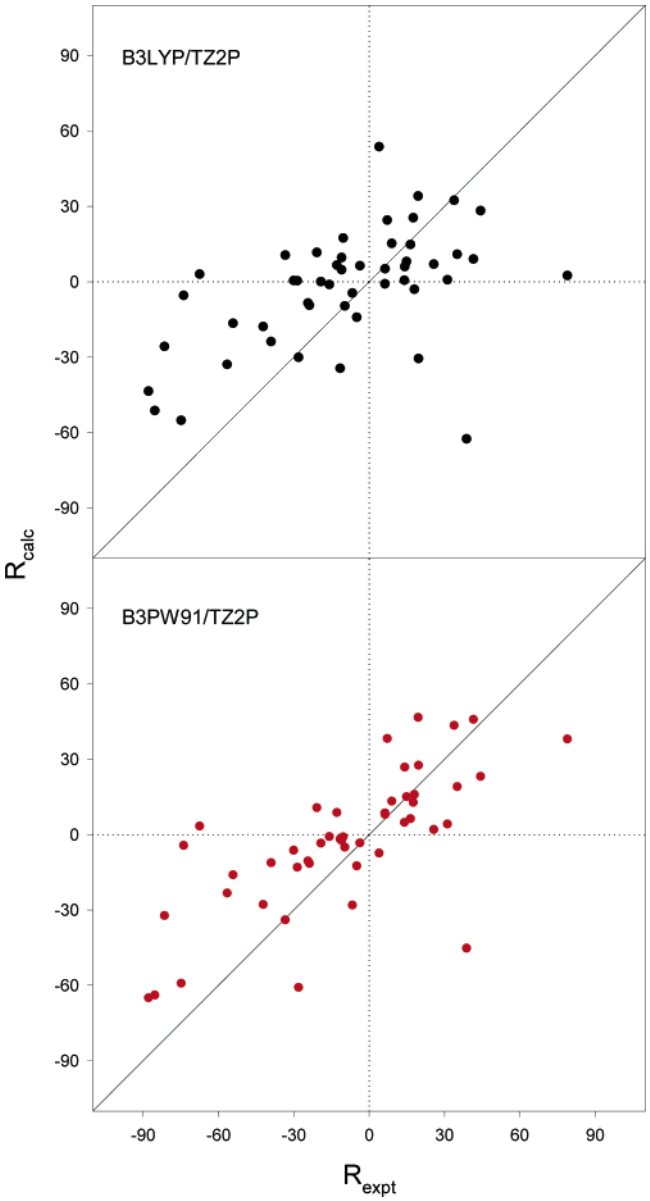


**FIGURE 11.** Comparison of calculated and experimental rotational strengths of **1**. Calculated rotational strengths are for (2*R*,7*S*,20*S*,21*S*)-**1** and are population-weighted averages. Experimental rotational strengths are for (+)-**1**. The solid line is of +1 slope. Rotational strengths are in units of $10^{-44}$ esu$^2$ cm$^2$.

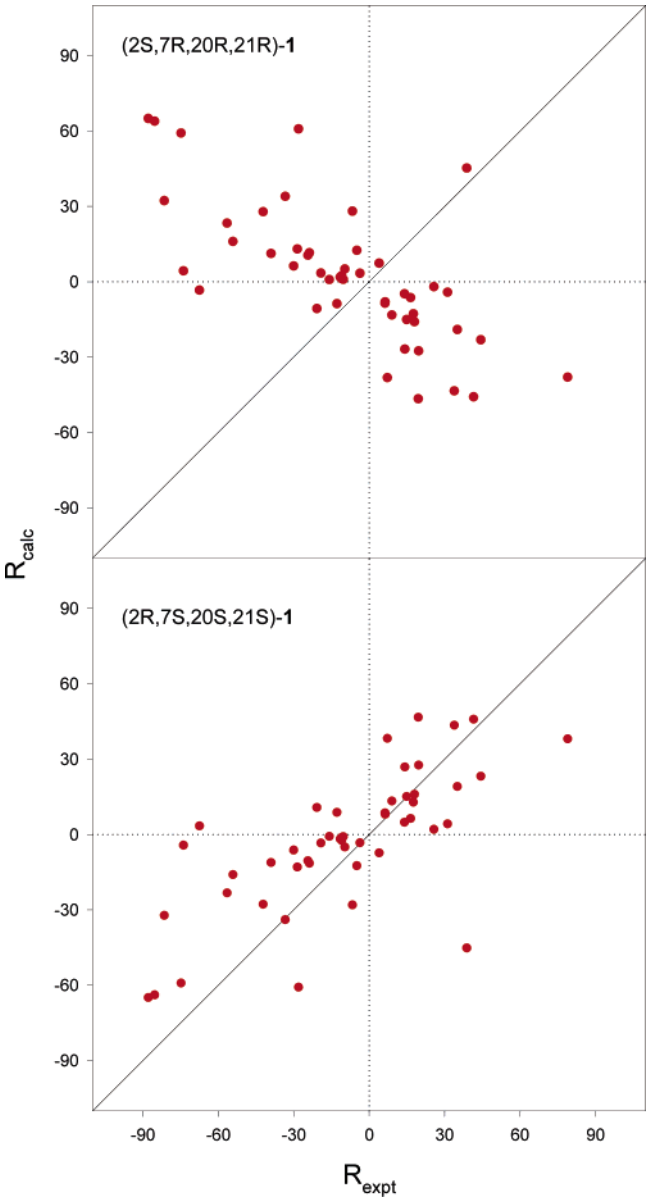


**FIGURE 12.** Comparison of experimental and B3PW91/TZ2P rotational strengths of **1**. Calculated rotational strengths are for (2*R*,7*S*,20*S*,21*S*)-**1** and (2*S*,7*R*,20*R*,21*R*)-**1** and are population-weighted averages. Experimental rotational strengths are for (+)-**1**. The solid line is of +1 slope. Rotational strengths are in units of $10^{-44}$ esu$^2$ cm$^2$.

signs respectively, in qualitative agreement with the experimental spectrum, which exhibits positive, negative, and positive features at 317, 268 and 232 nm. Consistent with the assignment of the UV spectrum, the positive feature at ~300 nm originates in excitations 1 of **1a**, **1a′**, **1b**, and **1b′** and the negative feature at ~270 nm originates in excitations 2−4. As shown in Figure 16, the conformationally averaged ECD spectrum predicted for (2*R*,7*S*,20*S*,21*S*)-**1** is more similar to the experimental spectrum of (+)-**1** than is the mirror-image spectrum predicted for (2*S*,7*R*,-20*R*,21*R*)-**1**, leading to the AC (2*R*,7*S*,20*S*,21*S*)-(+) for **1**, in agreement with the AC determined from the VCD spectrum.

**Specific Rotation.** The specific rotations of a 0.0116 M (*c* = 0.388) $CDCl_3$ solution of **1** have been measured at wavelengths 589, 578, 546, and 436 nm, with the results given in Table 2. The specific rotation is positive at all wavelengths, increasing monotonically with decreasing wavelength. $[\alpha]_D$ is +21.6, close to the value reported by Renner and Kernweisz, +15.5 (*c* = 1, $CHCl_3$).[1]

The specific rotations of the four conformations of (2*R*,7*S*,-20*S*,21*S*)-**1** have been calculated at the four wavelengths used experimentally, at the B3LYP/aug-cc-pVDZ level and with the B3LYP/6-31G*, B3LYP/TZ2P, and B3PW91/TZ2P geometries, with the results given in Table 2 and in Table 4 of the Supporting Information. At all wavelengths, the predicted rotation is not very sensitive to either the conformation or the geometry used. The conformationally averaged specific rotations are compared to the experimental rotations in Table 2, Table 4 of the Supporting Information, and Figure 17; the specific rotations for (2*S*,7*R*,20*R*,21*R*)-**1** are also plotted in Figure 17. It is clear that the calculated rotations are in much better agreement with experiment for the 2*R*,7*S*,20*S*,21*S* AC, further supporting the ACs derived from the VCD and ECD spectra.

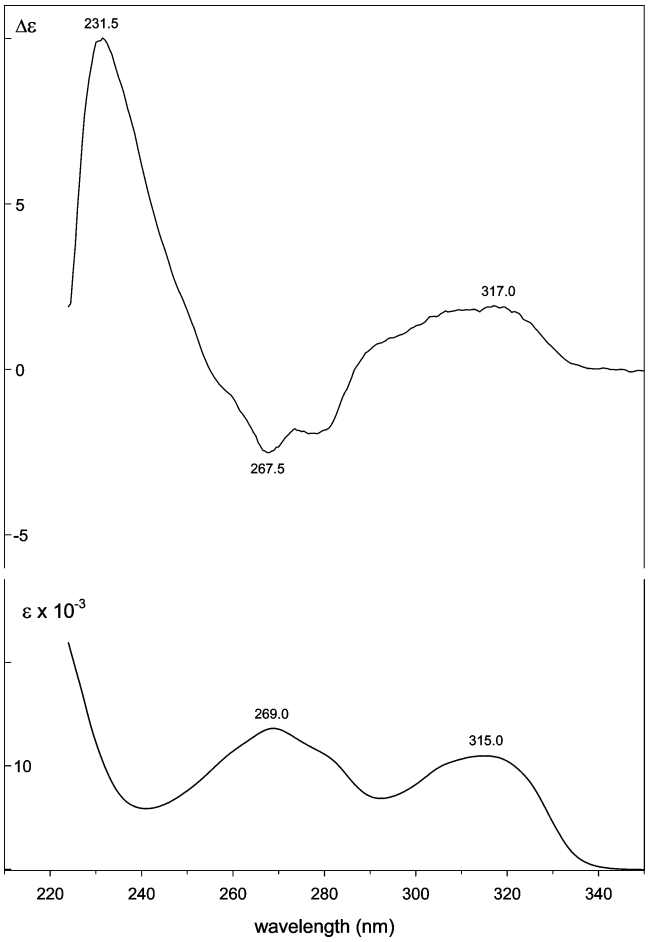


**FIGURE 13.** Experimental UV and ECD spectra of (+)-**1** in $CHCl_3$ solution at 12.5 mM and 100 $\mu$m path length.

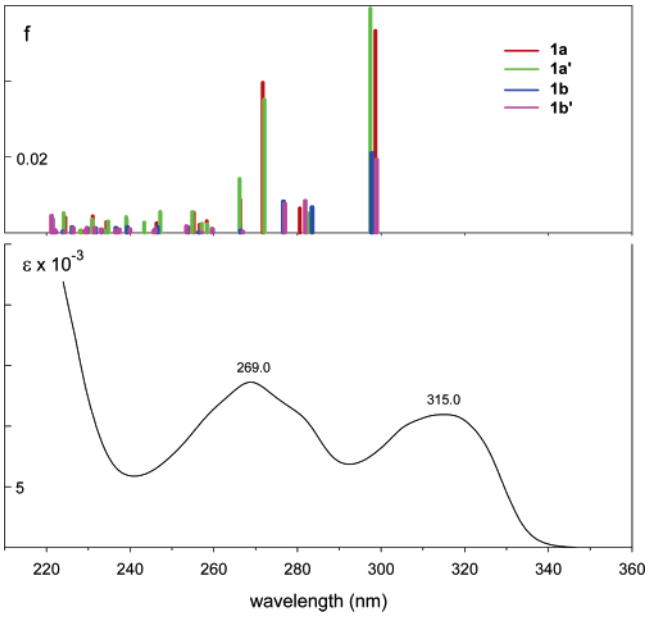


**FIGURE 14.** Comparison of B3LYP/aug-cc-pVDZ//B3PW91/TZ2P oscillator strengths of the conformations of **1** and the experimental UV spectrum. Oscillator strengths are population-weighted.

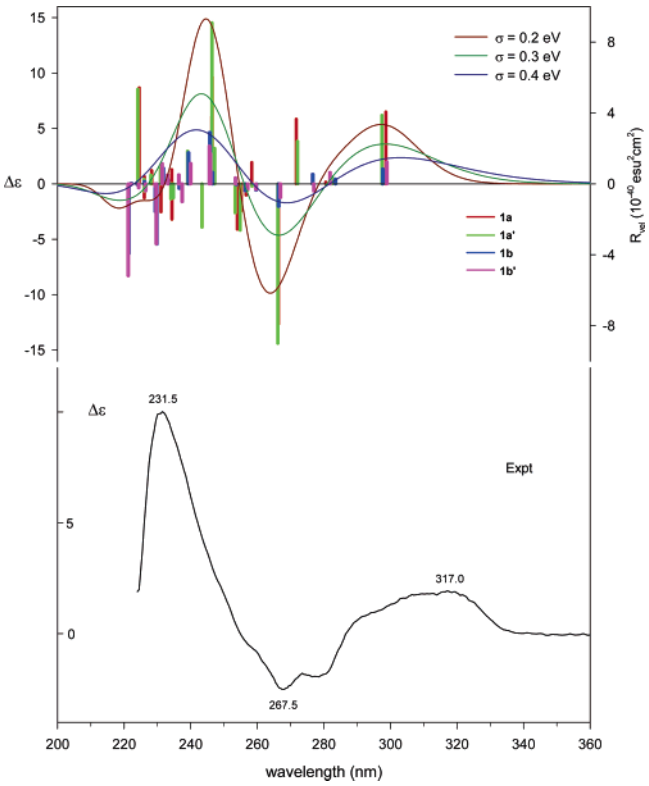


**FIGURE 15.** Comparison of B3LYP/aug-cc-pVDZ//B3PW91/TZ2P population-weighted velocity rotational strengths of the conformations of (2*R*,7*S*,20*S*,21*S*)-**1** and the conformationally averaged ECD spectra, simulated using Gaussian band shapes ($\sigma$ = 0.2, 0.3, and 0.4 eV), to the experimental ECD spectrum.

## Discussion

This work constitutes the second application of concerted DFT calculations of VCD, ECD, and OR to the determination of the AC of a natural product, the first being our recent study of the sesquiterpene quadrone,[24] and the first application to a natural product of previously unknown AC. All three chiroptical methods yield the same AC for **1**, (2*R*,7*S*,20*S*,21*S*)-(+), which is therefore unambiguously defined.

Since **1** is a conformationally flexible molecule, conformational analysis is prerequisite to DFT calculations of its VCD, ECD, and OR. In this work, we have followed the procedure used in prior conformational analyses,[21l−o,22,23f,24] in which the stable conformations are initially located via Monte Carlo searching with the MMFF94 molecular mechanics force field and their structures are subsequently reoptimized by DFT. Based on the DFT conformations, DFT potential energy surface (PES) scans are then carried out with respect to selected dihedral angles to evaluate the completeness of the MMFF94 conformational analysis. The importance of the last stage of this procedure is illustrated by our results for **1**: while only two conformations are located using MMFF94, DFT PES scans show that four conformations in fact exist.

Vibrational spectra are sensitive to the molecular geometry and, therefore, to the conformation. Accurate vibrational spectra of conformationally flexible molecules can therefore be predicted only when the conformational structures and populations are accurately predicted. Comparison of the conformationally averaged IR and VCD spectra of **1** to the corresponding experimental spectra thus enables the reliability of our conformational analysis of **1** to be evaluated. As shown in Figure 5,

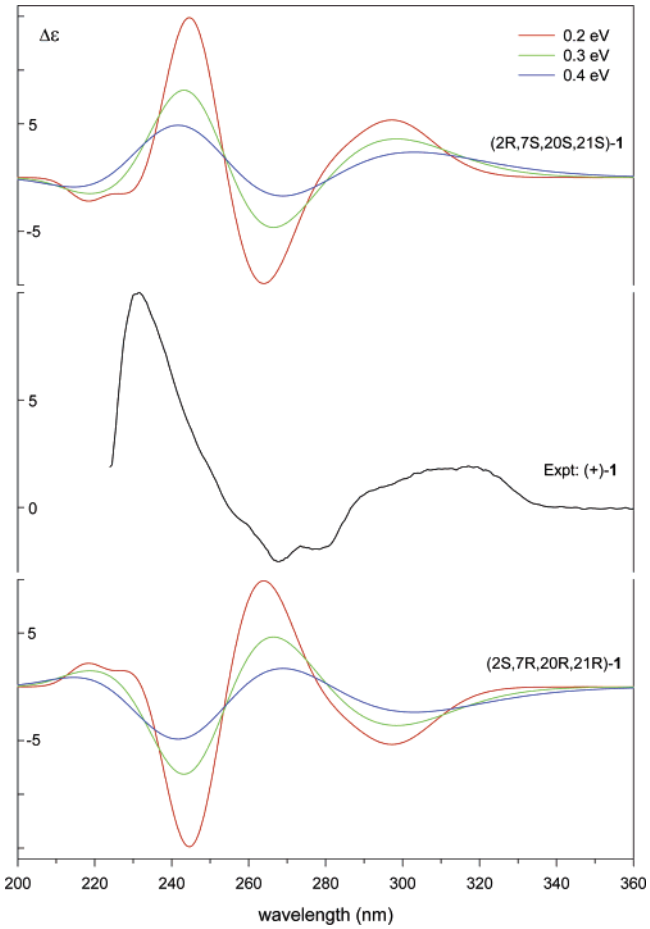


**FIGURE 16.** Comparison of the experimental and calculated ECD spectra of **1**. The experimental spectrum is for (+)-**1**. The calculated spectra are at the B3LYP/aug-cc-pVDZ//B3PW91/TZ2P level and are simulated using Gaussian shapes with $\sigma = 0.2$, 0.3, and 0.4 eV.

**TABLE 2. Comparison of the Calculated[a] and Experimental Specific Rotations[b] of (2*R*,7*S*,20*S*,21*S*)- and (+)-1**

| conformer | $[\alpha]_D$ | $[\alpha]_{578}$ | $[\alpha]_{546}$ | $[\alpha]_{436}$ |
|---|---|---|---|---|
| **1a** | 34.01 | 36.40 | 44.79 | 118.53 |
| **1a′** | 51.36 | 54.50 | 65.28 | 150.66 |
| **1b** | 46.13 | 49.22 | 59.92 | 147.47 |
| **1b′** | 38.92 | 41.79 | 51.88 | 140.09 |
| avg[c] | +42.75 | +45.58 | +55.41 | +137.33 |
| expt | +21.63 | +23.95 | +28.33 | +73.40 |

[a] At the B3LYP/aug-cc-pVDZ//B3PW91/TZ2P level. [b] Specific rotations in degrees $[dm \cdot g/cm^3]^{-1}$. [c] Population-weighted average.

the B3PW91/TZ2P IR spectrum is in excellent agreement with the experimental IR spectrum, permitting a detailed assignment of the latter over the range 400−1800 $cm^{-1}$. Most importantly, as discussed in detail above, bands originating in either conformations **la**/**1a′** or **1b**/**1b′** alone are resolved, with relative intensities consistent with the intensities predicted using the B3PW91/TZ2P relative free energies. If the experimental conformations were substantially different in number, structures, and relative free energies from our predicted conformations, the predicted IR spectrum would be in much poorer agreement with experiment. The quality of the agreement observed strongly supports the reliability of the conformational analysis of **1**. Of course, the agreement of calculated and experimental IR spectra is not perfect. Quantitative evaluation of the agreement is provided by comparison of the experimental frequencies and dipole strengths obtained via Lorentzian fitting of the IR spectrum to the calculated values. As shown in Figure 6, except for a few very low-frequency modes, calculated frequencies are systematically greater than experimental frequencies. As is well-known,[30] the errors in the calculated frequencies originate predominantly in the neglect of anharmonicity in the vibrational force field. To a lesser extent, errors also arise from the neglect of solvent effects and from the inexactness of the density functional used. In the case of the dipole strengths, the deviations between calculated and experimental values can be attributed not only to the neglect of anharmonicity and solvent effects and the imperfection of the functional but also to the inexactness of the calculated conformational relative free energies and equilibrium populations.

The assignment of the IR spectrum of **1** leads automatically to the assignment of the VCD spectrum, since every vibrational transition contributing to the VCD spectrum occurs at a frequency identical to that of the corresponding transition in the IR spectrum. Comparison of the experimental VCD spectrum of (+)-**1** with the predicted VCD spectrum for the two enantiomers of **1** then leads to the AC of (+)-**1**. As shown in Figure 10, with very few exceptions, the signs of the VCD intensities for (2*R*,7*S*,20*S*,21*S*)-**1** are in agreement with the experimental signs for the corresponding transitions. For the same transitions, the signs for (2*S*,7*R*,20*R*,21*R*)-**1** are in disagreement. It follows that the AC of **1** must be (2*R*,7*S*,20*S*,-21*S*)-(+). Lorentzian fitting of the experimental VCD spectrum gives the experimental rotational strengths of the observed transitions of (+)-**1**. Comparison to the calculated rotational strengths for the two enantiomers of **1**, shown in Figure 12, clearly confirms the superior agreement for the 2*R*,7*S*,20*S*,21*S* enantiomer. As with the dipole strengths, and for the same reasons, quantitative agreement of calculated and experimental rotational strengths is not perfect. However, the errors are very much larger for the 2*S*,7*R*,20*R*,21*R* enantiomer, eliminating any possibility that this is the AC of (+)-**1**.

Comparison of the predicted ECD spectra for the two enantiomers of **1** to the experimental spectrum provides further support for the AC determined from the VCD spectrum. The predicted ECD spectrum of (2*R*,7*S*,20*S*,21*S*)-**1** exhibits three bands with +, −, and + signs over the range 220−360 nm, in qualitative agreement with the experimental spectrum of (+)-**1**. For the AC 2*S*,7*R*,20*R*,21*R* each band is opposite in sign to that observed experimentally. Agreement for the 2*R*,7*S*,20*S*,-21*S* AC is not perfect, however. Predicted and experimental peak wavelengths are not identical, principally due to the imperfection of the B3LYP functional. Predicted and experimental band shapes and peak $\Delta\epsilon$ values differ, which can be attributed to a variety of sources: the assumption that all excitations have Gaussian band shapes of identical width, errors in calculated rotational strengths due to imperfection of the B3LYP functional, and errors in the predicted conformational populations.

Comparison of the analysis of the VCD and ECD spectra of **1** clearly demonstrates the greater reliability of the AC deduced from the VCD spectrum. The vibrational transitions observed are far more numerous than the electronic transitions and, in addition, far more highly resolved, due to their much smaller bandwidths. As a result, it is possible to compare the calculated and experimental CD of far more vibrational bands than electronic bands. Further, because the shapes of the vibrational transitions are Lorentzian, experimental rotational strengths can

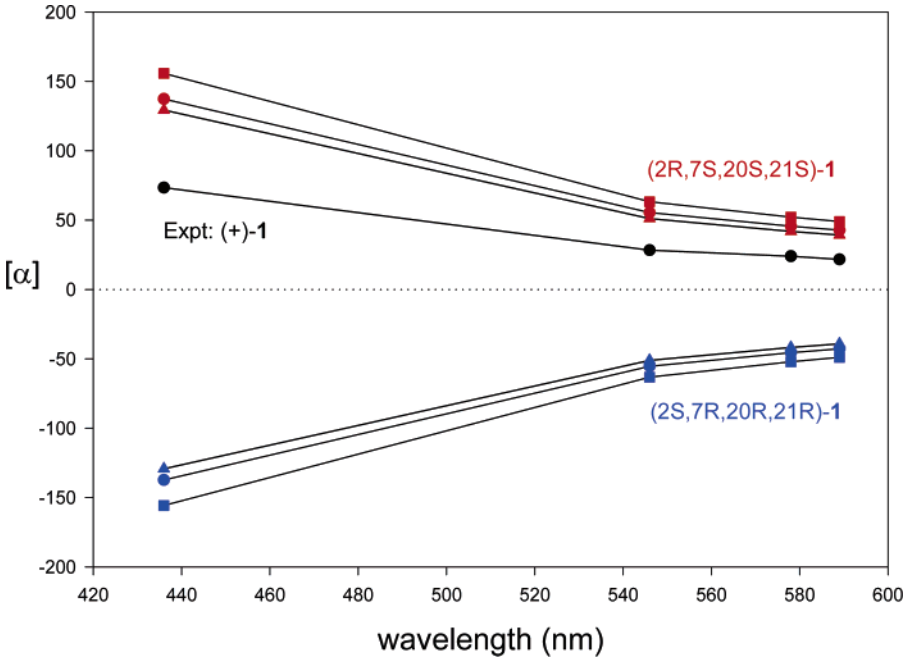


**FIGURE 17.** Comparison of experimental and calculated specific rotations of **1**. The experimental data are for (+)-**1**. The specific rotations are calculated at the B3LYP/aug-cc-pVDZ level using B3LYP/6-31G* (■), B3LYP/TZ2P (▲), and B3PW91/TZ2P (●) geometries.

**TABLE 3. Calculated Relative Energies (Δ*E*),[a] Relative Free Energies (Δ*G*),[a] and Percentage Populations (*P*)[b] of the Conformers of 2**

| | MMFF94 | B3LYP/6-31G* | | |
|---|---|---|---|---|
| conformer | Δ*E* | Δ*E* | Δ*G* | *P*[b] (%) |
| **2a** | 0.00 | 0.00 | 0.00 | 69.70 |
| **2b** | 1.92 | 0.33 | 0.49 | 30.30 |
| **2c** | 8.15 | 6.66 | 5.90 | 0.00 |
| **2d** | 9.02 | 7.17 | 7.93 | 0.00 |
| **2e** | 9.93 | 7.48 | 7.06 | 0.00 |
| **2f** | 18.44 | 12.27 | 12.31 | 0.00 |

[a] In kcal/mol. [b] Population calculated based on Δ*G* at $T = 298.15$ K.

be extracted from the experimental VCD spectrum via Lorentzian fitting, permitting quantitative comparison of calculated and experimental vibrational rotational strengths. In view of the uncertain shapes of the electronic transitions, this is not the case for electronic rotational strengths. Overall, therefore, the determination of ACs from VCD spectra is based on more transitions, is more quantitative, and is consequently more reliable than is the determination of ACs from the ECD spectra.

The use of transparent spectral region optical rotations at a small number of wavelengths to determine ACs is procedurally much simpler than the use of VCD and ECD spectra. All that needs to be done is to compare the signs and magnitudes of predicted and experimental specific rotations at each wavelength and the shapes of the predicted and experimental dispersions (wavelength dependences). As seen in Figure 17, for (+)-**1** the predicted specific rotations from 589 to 436 nm for (2*R*,7*S*,20*S*,21*S*)-**1** are in much better agreement than those predicted for the 2*S*,7*R*,20*R*,21*R* AC, providing further support for the (2*R*,7*S*,20*S*,21*S*)-(+) AC deduced from the VCD and ECD spectra. Most strikingly, the monotonically increasing positive rotation with decreasing wavelength observed experimentally is perfectly reproduced qualitatively. Quantitative agreement is not perfect: calculated rotations overestimate the experimental rotations at all wavelengths. Given the quantitative reliability of specific rotations previously calculated by use of the TDDFT methodology at the B3LYP/aug-cc-pVDZ level,[23b,31] the results for **1** are not unexpected. The errors can be attributed to the imperfection of the B3LYP functional, the neglect of vibrational contributions, and/or the neglect of solvent effects.

As discussed above, the AC of the closely related alkaloid strempeliopine, **2**, whose specific rotation at 578 nm is negative, has been shown to be 2*S*,7*R*,20*R*,21*R*, opposite to that we have assigned to (+)-**1**. In order to further evaluate the reliability of our calculations of the specific rotations of **1**, we have also carried out calculations for **2**. The results of the conformational analysis of **2** using MMFF94 and DFT at the B3LYP/6-31G* level are given in Table 3. Six conformations, **2a**−**f**, are found using MMFF94 Monte Carlo searching, within a 20 kcal/mol window. At the B3LYP/6-31G* level, the energy and free energy of only one of these conformations, **2b**, is within 5 kcal/mol of the lowest energy conformation, **2a**. As a result, only two conformations, **2a** and **2b**, are predicted to be significantly populated. The B3LYP/6-31G* structures of conformations **2a**−**f** are shown in Figure 18. The dihedral angles of rings B−E of **2a**−**f** are compared to the corresponding angles of conformations **a**, **a′**, **b**, and **b′** of **1** in Table 5 of the Supporting Information. The conformations of rings B, C, and D of **2a** and **2b** are similar to those in **1a**/**1a′** and **1b**/**1b′**, respectively. As is to be expected, the conformations of ring E of **2a** and **2b** differ substantially from those in **1a**, **1a′**, **1b**, and **1b′**; in both **2a** and **2b**, ring E exhibits a chair conformation. The specific rotations of **2a** and **2b** at the sodium D line and at 578 nm are given in Table 4 for the 2*S*,7*R*,20*R*,21*R* AC. In contrast to the low-energy conformations of **1**, the specific rotations of **2a** and **2b** vary in sign. $[\alpha]_D$ and $[\alpha]_{578}$ of (2*S*,7*R*,20*R*,21*R*)-**2a** are negative and considerably larger than the positive rotations of (2*S*,7*R*,20*R*,-21*R*)-**2b**. As a result, the predicted conformationally averaged $[\alpha]_D$ and $[\alpha]_{578}$ values are negative in sign. $[\alpha]_{578}$ is −17.15, in

(31) Stephens, P. J.; McCann, D. M.; Cheeseman, J. R.; Frisch, M. J. *Chirality* **2005**, *17*, S52−S64.

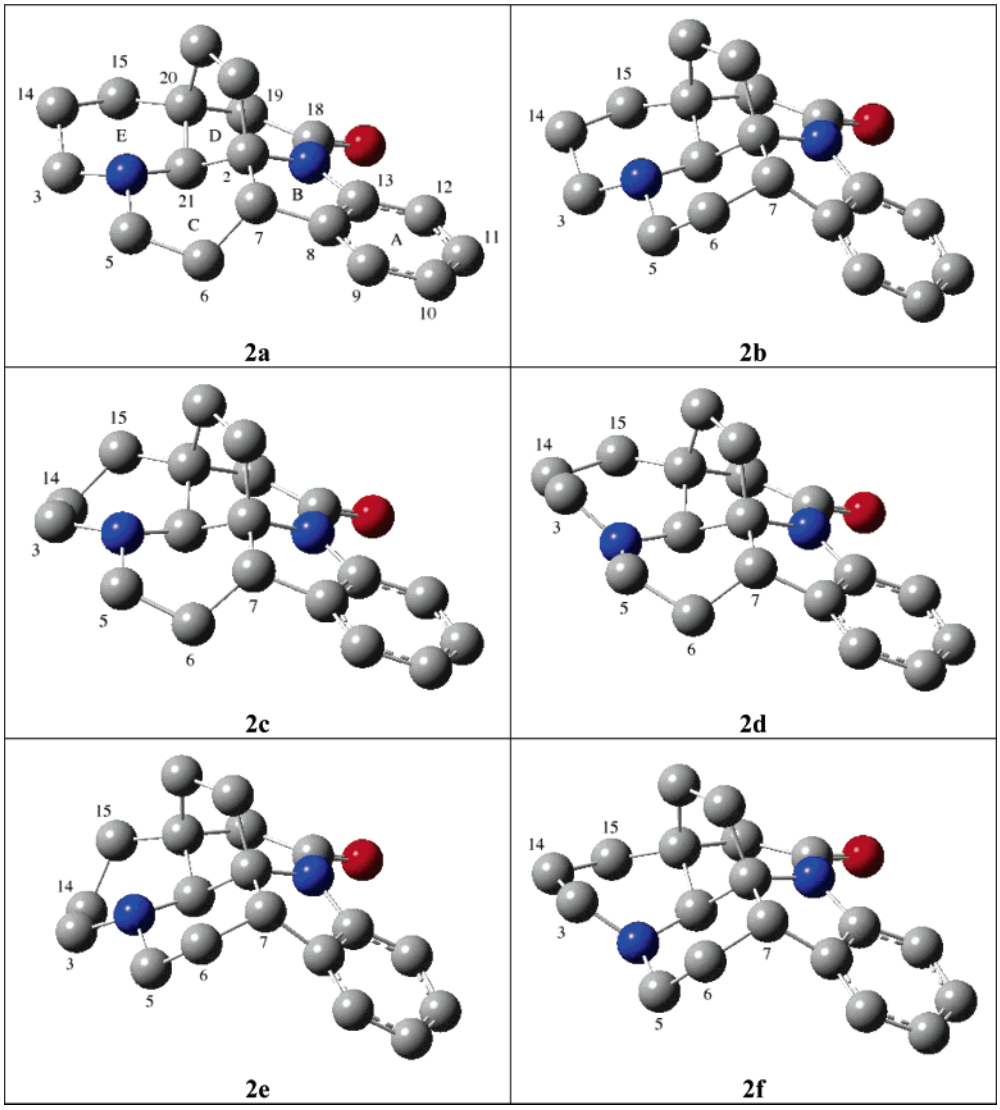


**FIGURE 18.** B3LYP/6-31G* structures of the conformations **2a**−**f**.

**TABLE 4. Comparison of the Calculated[a] and Experimental Specific Rotations[b] of (2*S*,7*R*,20*R*,21*R*)- and (+)-2**

| conformer | $[\alpha]_D$ | $[\alpha]_{578}$ |
|---|---|---|
| **2a** | −28.99 | −30.65 |
| **2b** | +13.42 | +13.90 |
| avg[c] | −16.14 | −17.15 |
| expt[d] | | −25.40 |

[a] At B3LYP/aug-cc-pVDZ//B3LYP/6-31G* level. [b] Specific rotations are given in degrees [decimeter·gram per cubic centimeter]$^{-1}$. [c] Population-weighted average. [d] From ref 11.

good agreement with the experimental value of −25.4. This result provides further support for the reliability of the TDDFT methodology used in this paper to calculate optical rotations.

Alkaloids closely related in structure to schizozygine have been isolated from *Schizozygia caffaeoides*, including schizogaline, **3**, and schizogamine, **4**, which differ from **1** only in the substitution pattern of ring A.[1,2] The specific rotations $[\alpha]_D$ of **3** and **4** are +28.8 ($CHCl_3$) and −7.9 ($CHCl_3$), respectively.[1] Assuming that the biosynthetic pathways to **1**, **3**, and **4** are identical in this plant, it can be concluded that the ACs of the naturally occurring (+)-**3** and (−)-**4** are also 2*R*,7*S*,20*S*,21*S*.

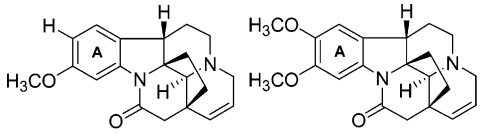

**3** **4**

Very recently, a new schizozygane alkaloid, 6,7-dehydro-19$\beta$-hydroxyschizozygine, **5**, has been isolated from *S. caffaeoides*.[5] If it is assumed that the biosynthetic pathways to **1** and **5** are identical, it can be concluded that the AC of naturally occurring **5** is 2*R*,19*R*,20*S*,21*S*.

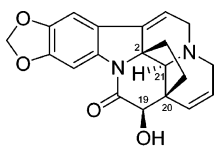

**5**

The structures of the schizozygane alkaloids isoschizogaline, **6**, and isoschizogamine, **7**, are significantly different from those

of **3** and **4**;[5−7] although a biosynthetic pathway to **7** has been

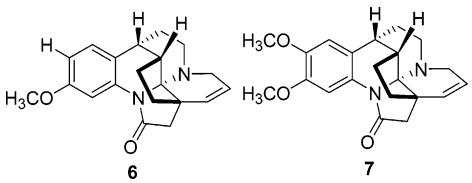

**6** **7**

proposed,[6] their ACs are less reliably deduced by analogy to the ACs of **1**, **3**, and **4**. Independent determinations of their ACs by the methods of this paper are currently underway and will be reported in the near future.

**Acknowledgment.** We are grateful for financial support from the National Science Foundation (to P.J.S., Grants CHE-0209957 and CHE-0614577) and from the Ministry of Education, Youth and Sports of the Czech Republic (to M.U., Grant MSM6046137307). We also thank the USC High Performance Computing and Communication (HPCC) facility for computer time, Hewlett-Packard for the use of an Alpha server (ES45) HP computer, Dr. J. R. Cheeseman of Gaussian Inc. for his continual assistance and advice, and Dr. O. Julínek for assistance with the ECD measurements.

**Supporting Information Available:** PES scans; dihedral angles of calculated geometries; experimental and calculated IR and VCD spectra and vibrational frequencies, dipole strengths, and rotational strengths; Lorentzian fits of IR and VCD spectra; calculated electronic excitation energies, oscillator strengths, rotational strengths, and ECD spectra; and calculated specific rotations. This material is available free of charge via the Internet at http://pubs.acs.org.

JO062567P